Published in final edited form as:

Cell Rep. 2023 November 28; 42(11): 113294. doi:10.1016/j.celrep.2023.113294.

Bordetella spp. block eosinophil recruitment to suppress the generation of early mucosal protection

Nicholas J. First[1,6], **Katelyn M. Parrish**[1,6], **Amparo Martínez-Pérez**[2,6], **África González-Fernández**[2,6], **Sushma Bharrhan**[1,3], **Matthew Woolard**[1,3], **James B. McLachlan**[4], **Rona S. Scott**[1,5], **Jian Wang**[1,5], **Monica C. Gestal**[1,7,*]

[1]Department of Microbiology and Immunology, Louisiana State University Health Sciences Center at Shreveport, Shreveport, LA 71106, USA

[2]CINBIO, Universidade de Vigo, Immunology Group, Instituto de Investigación Sanitaria Galicia Sur (IIS Galicia Sur), SERGAS-UVIGO, 36310 Vigo, Galicia, Spain

[3]Immunophenotyping Core, Center for Applied Immunology and Pathological Processes, Department of Microbiology and Immunology, Louisiana State University Health Sciences Center at Shreveport, Shreveport, LA 71106, USA

[4]Department of Microbiology and Immunology, Tulane University School of Medicine, New Orleans, LA 70112, USA

[5]Bioinformatics and Modeling Core, Center for Applied Immunology and Pathological Processes, Department of Microbiology and Immunology, Louisiana State University Health Sciences Center at Shreveport, Shreveport, LA 71106, USA

[6]These authors contributed equally

[7]Lead contact

SUMMARY

Bordetella spp. are respiratory pathogens equipped with immune evasion mechanisms. We previously characterized a *Bordetella bronchiseptica* mutant (RB50Δ*btrS*) that fails to suppress host responses, leading to rapid clearance and long-lasting immunity against reinfection. This work revealed eosinophils as an exclusive requirement for RB50Δ*btrS* clearance. We also show that RB50Δ*btrS* promotes eosinophil-mediated B/T cell recruitment and inducible bronchus-

*Correspondence: monica.cartellegestal@lsuhs.edu.

AUTHOR CONTRIBUTIONS

N.J.F., *in vivo* experiments, visualization, data curation, and contributions to writing and editing; K.M.P., brainstorming, validation, formal analysis, investigation, and writing and editing; A.M.-P., brainstorming, formal analysis, and contributions to writing and editing; A.G.-F., brainstorming, formal analysis, and contributions to writing and editing; S.B., experiments, formal analysis, and editing; M.W., brainstorming, formal analysis, and editing; J.B.M., brainstorming, visualization, and writing and editing; R.S.S., design of RNA sequencing experiments and software, data analysis, and editing; J.W., genomic data analysis and contributions to software development; M.C.G., project conceptualization, experimental design, experiments, formal analyses, validation, visualization, resources, writing and editing, funding, project administration, and supervision.

SUPPLEMENTAL INFORMATION

Supplemental information can be found online at https://doi.org/10.1016/j.celrep.2023.113294.

DECLARATION OF INTERESTS

The authors declare no competing interests.

associated lymphoid tissue (iBALT) formation, with eosinophils being present throughout iBALT for Th17 and immunoglobulin A (IgA) responses. Finally, we provide evidence that XCL1 is critical for iBALT formation but not maintenance, proposing a novel role for eosinophils as facilitators of adaptive immunity against *B. bronchiseptica.* RB50Δ*btrS* being incapable of suppressing eosinophil effector functions illuminates active, bacterial targeting of eosinophils to achieve successful persistence and reinfection. Overall, our discoveries contribute to understanding cellular mechanisms for use in future vaccines and therapies against *Bordetella* spp. and extension to other mucosal pathogens.

Graphical Abstract

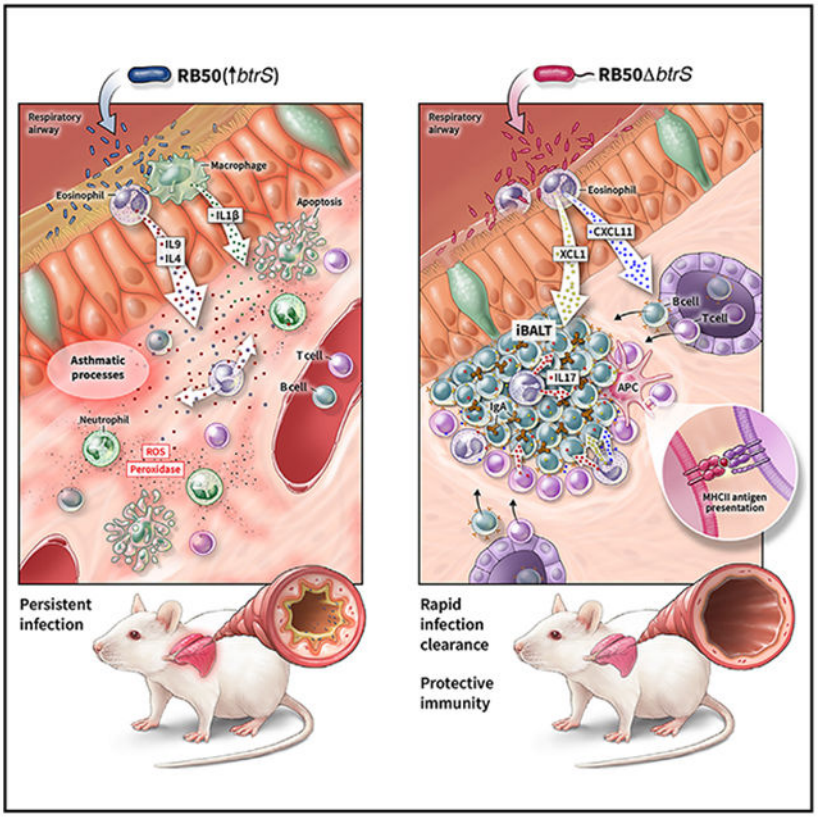

In brief

First et al. elucidate a *btrS*-mediated mechanism utilized by *B. bronchiseptica* to hinder eosinophil effector functions. Eosinophils drive iBALT formation within 7 days following *btrS*-null infection, fostering Th1/Th17 cellular responses and IgA-mediated humoral immunity. These findings introduce a potential role of eosinophils in shaping adaptive mucosal immune responses during respiratory infections.

INTRODUCTION

Infectious diseases are a contributing factor to worldwide morbidity, mortality, and disability.[1] Although the development of vaccines[2] and therapies[3] have aided in controlling

them, new and old diseases continue to arise,[4] including those caused by the *Bordetella* spp.[5] *Bordetella* spp. are respiratory bacterial pathogens responsible for whooping cough, a long-term persistent infection characterized by high mortality in infants.[6,7] The prevalence of infection in newborns under 6 months of age is estimated to be 72.3 for every 100,000 inhabitants in the United States,[8] but resurging cases and outbreaks have been reported worldwide.[9-12] Pertussis-associated pneumonia in approximately 32% of reported neonatal cases can result in fatal pulmonary hypertension.[13-15] The classic *Bordetella* group[16] consists of the human-exclusive pathogen *Bordetella pertussis*; *Bordetella parapertussis,* which infects humans and sheep; and *Bordetella bronchiseptica,* which causes disease in a wide variety of mammals,[17,18] including mice and humans.[19] *B. bronchiseptica* is considered an evolutionary ancestor[20] of the two human-specific species because of the high identity of shared genetic content.[17,21,22] *Bordetella* spp. use conserved host immune evasion strategies,[18,23-25] including phagocyte manipulation.[26-29] In the natural host, pathogens can cause disease following inoculation with low infectious doses, observed with *B. pertussis* infection in humans and *B. bronchiseptica* infections in mice.[30] However, *B. pertussis* infection in mice requires a higher inoculum for disease to develop[31] and is only capable of causing acute disease, jeopardizing the central damage-response framework[32,33] and physiological relevance of this infection model. Thus, evolutionary homology among the classic *Bordetella* spp. as well as the similarities in disease progression allow mechanistic studies of host-pathogen interactions at the cellular and molecular level[34] using *in vivo* infection models with *B. bronchiseptica.*

Investigating how *Bordetella* spp. suppress host immune responses led to the discovery of *btrS,* which encodes a highly conserved sigma factor that regulates several bacterial immunosuppressive pathways.[35] Mice challenged with a *B. bronchiseptica* RB50[36] mutant lacking *btrS* (RB50Δ*btrS*[37,38]) rapidly cleared the bacteria from the lungs and generated a response that completely protected the mice from reinfection with *B. bronchiseptica*, *B. pertussis*, and *B. parapertussis*.[39] Lastly, we discovered an essential role of eosinophils in the development of an effective adaptive immune response during infection with RB50Δ*btrS*.[40]

Eosinophils are granulocytes that protect against parasitic infections and can contribute to allergic and asthmatic reactions.[41] These cells are likely evolutionarily preserved to serve protective functions beyond their pathogenic roles.[42-44] A protective role of eosinophils in immune responses against bacterial infections was proposed in 1970; the study demonstrated that eosinophils, similarly to neutrophils, can colocalize with bacteria and facilitate killing.[45] But only recently have researchers shown a role of eosinophils during *Helicobacter pylori* infection in dampening proinflammatory responses, leading to increased bacterial persistence in the gastrointestinal tract.[46] A protective role of these cells has also been noted during *Mycobacterium tuberculosis* infection[47] and vaccination, having an integral and regulatory role in antibody production during vaccine responses.[48] It has been established that pertussis disease can lead to the development of asthma and allergies,[7,49] even at sub-clinical colonization levels.[49] Recently, researchers have also shown that use of the live-attenuated *Bordetella* vaccine BPZE1 improves the outcome and symptoms of eosinophilic disorders.[50,51] When investigating the role of eosinophils during respiratory infections with RB50Δ*btrS*, we found that the absence of eosinophils leads to prolonged infection[40] and

contributes to the formation of a structure that resembles lymphoid aggregates adjacent to lung bronchi.[40]

In this study, we explored the role of eosinophils in the generation of adaptive mucosal immune responses to *B. bronchiseptica*. We used two different models of eosinophil-deficient mouse strains that have been validated previously by several studies of eosinophilic esophagitis[52,53] as well as in our own study (Figure S1A). The first model includes BALB/c wild-type and eosinophil-deficient ΔdblGATA-1[54] strains containing a mutation in the GATA-1 gene leading to an ablation of the eosinophil lineage.[52] Our secondary model combines C57BL/6J and eosinophil-deficient *EPX/MBP*$^{-/-}$ mice,[53] in which the mutation specifically targets eosinophil peroxidase (EPX) and the major basic protein (MBP). Using these two models, our goals were to evaluate the contributions of eosinophils in the generation of Th1/Th17 responses, early formation of inducible bronchus-associated lymphoid tissue (iBALT), and overall bacterial persistence in the lungs. Understanding the mechanisms that bacteria utilize to suppress eosinophil effector functions to dampen adaptive immune responses can provide novel avenues for vaccine and therapeutic development that are still to be discovered.

RESULTS

Eosinophils are required for clearance of RB50Δ*btrS* but not RB50

We have shown previously that clearance of RB50Δ*btrS* is dependent on eosinophils.[40] Interestingly, *btrS* is conserved among *Bordetella* spp. (99.5%) and other pathogens,[35] including *Yersinia pestis* and *Pseudomonas aeruginosa* (Figure S1B), suggesting that it might have similar immunosuppressive mechanisms. To explore the role of eosinophils during infection with *B. bronchiseptica,* we challenged BALB/c and ΔdblGATA-1 mice and C57BL/6J and *EPX/MBP*$^{-/-}$ mice with the RB50 or RB50Δ*btrS* strains and then enumerated colonies at different times post infection (Figures 1A, 1B, and S2A). We focused on day 14, which corresponded with the day when infection with RB50Δ*btrS* is cleared from the lungs (Figures 1A and 1B).

There were no significant differences in bacterial burden or the clearance dynamics of RB50 in the presence or absence of eosinophils (Figures 1A and S2A; Table 1), suggesting that eosinophils do not contribute to bacterial clearance during RB50 infection and that eosinophil effector functions may be blocked via a *btrS*-mediated mechanism. Contrary to wild-type mice, we observed a delayed clearance of RB50Δ*btrS* from the lungs in both eosinophil-deficient mouse models (Figures 1B and S2A; Table 1). These results indicate an important role of eosinophils during the clearance of RB50Δ*btrS* that is absent in RB50 infection, possibly because of a bacterial mechanism that suppresses eosinophil-mediated clearance during wild-type infection. From these results, we concluded that the role of eosinophils during bacterial infections may be masked by the ability of these well-adapted pathogens to manipulate these cells.

btrS blocks transcriptional changes associated with adaptive immune responses in an eosinophil-dependent manner

We have seen that infection with RB50Δ*btrS* leads to increased numbers of B/T cells and Th1/Th17 mucosal responses in the lungs of wild-type mice as early as 14 days post infection.[38,39] It is well established that Th17 responses are required for protection against *Bordetella* spp. infection.[55] The immunological transcriptional signatures associated with protection revealed that vaccinated mice have a decrease in the mRNA levels of pathways involved in neutrophil recruitment or interleukin-6 (IL-6) responses, correlating these transcriptomic signatures with protection against disease[56,57]. Our results indicate delayed clearance in the absence of eosinophils, leading us to hypothesize that *btrS* expression blocks host inflammatory signaling cascades that become activated through eosinophils. To test this hypothesis, bulk lung RNA sequencing was performed to assess transcript abundance and identify specific signatures of wild-type or eosinophil-deficient mice infected with RB50 or RB50Δ*btrS*. We wanted to investigate immunological transcriptional signatures that were from host-specific responses and not from differential bacterial burden. Thus, we performed our studies on day 7 post infection, when differences in bacterial burden between mouse models were insignificant (Figure S2B), confirming that observed differences were exclusively attributable to alterations in the host immune response.

Principal-component analysis (PCA) (Figure S2C) revealed a trend of samples of the same type of infection to cluster together, suggesting similar transcriptomic signatures caused by each specific bacterial infection. The blind analyses were restricted to genes with a significance p value of 0.05 or greater and absolute $\log_2$ fold change of 1.5 or greater compared with uninfected controls. A total of 1,512 differentially expressed genes (DEGs) were identified in BALB/c mice infected with the wild-type strain RB50 (Figures 1C and S2D) compared with uninfected mice. RB50Δ*btrS*-infected mice presented 3,231 DEGs, suggesting a more active transcriptional response to infection. In ΔdblGATA-1 mice, the number of DEGs was significantly lower, with 990 in the ΔdblGATA-1 mice infected with RB50 and 1,725 with RB50Δ*btrS*. When comparing BALB/c and GATA-1 mouse responses, the number of DEGs was significantly lower in ΔdblGATA-1 mice following infection with either of the bacterial strains (Figures 1C and S2D).

To better understand the physiological meaning of these changes, we performed a gene set enrichment analysis, which revealed a high participation of all groups in multiple pathways involving adaptive responses, including leukocyte activation, migration, and cytokine production (Figure 1D). However, there seemed to be a lesser presence of the lymphocytic T cell response in BALB/c mice infected with RB50 wild-type bacteria. Based on our phenotypic data, we expected fewer differences among ΔdblGATA-1 mice. Instead, we found upregulation of multiple routes related to lymphocytic responses in both ΔdblGATA-1 groups and in BALB/c mice infected with RB50Δ*btrS*. Our results indicated that challenge with RB50Δ*btrS* leads to a more robust lymphocyte response and active antigen presentation as well as a general upregulation of T and B cell activation (Figure 1D). Although we also observed an increase in antigen presentation transcriptomic markers after infection of the ΔdblGATA-1 mice, many other pathways that appeared to be enhanced in the RB50Δ*btrS* BALB/c infection were not increased in these mice, suggesting that,

although the enhanced antigen presentation might play a role in the rapid clearance of the RB50Δ*btrS* strain, there might also be an effect of cytokines or chemokines that can contribute to the increased lymphocyte response observed.

Overall, our transcriptomics analysis suggests that, in wild-type mice, *btrS* suppresses the expression of genes associated with leukocyte and lymphocyte activation as well as antigen presentation. Thus, eosinophils appear to be important for the enhancement of the immune responses, but their functions are suppressed by *btrS* during infection with the wild-type strain.

B. bronchiseptica suppresses adaptive immune responses via the *btrS* signaling pathway in an eosinophil-dependent manner

Based on our transcriptomics results, we hypothesized that *btrS* blocks the early recruitment of eosinophils to the lungs to suppress the generation of rapid adaptive immune responses. A heatmap analysis selected for surface markers and cytokines associated with T cells was performed (Figure 2A). In BALB/c mice, lungs infected with RB50Δ*btrS* revealed increased transcript levels of genes associated with $CD4^+$ and $CD8^+$ T cells, including but not limited to tumor necrosis factor alpha (TNF-α), IL-6, interferon gamma (IFN-γ), chemokine (C-C motif) ligand 19 (CCL19), and IL-17, in line with our pathway analysis. We also detected higher levels of TNF-α and IL-6 in RB50-infected lungs compared with uninfected controls. In ΔdblGATA-1 mice, the number of transcripts associated with markers of $CD4^+$ cells after infection with the RB50 strain was substantially decreased. ΔdblGATA-1 mice presented a reduction in the numbers of transcripts associated with $CD8^+$ T and B cells. To validate our findings, we performed qRT-PCR using coded samples to blindly analyze the contribution of eosinophils (Figure S2E). Our results showed that these genes were significantly increased in BALB/c and C57BL/6J mice after infection with RB50Δ*btrS* but not with RB50. Overall, these data suggest that, in wild-type mice, *B. bronchiseptica* suppresses the expression of genes associated with adaptive immune responses through a *btrS*-associated mechanism that requires eosinophils.

Next, we evaluated B and T cell recruitment to the lungs at 7 days post-infection (dpi). Flow cytometry of blinded coded samples was used as a primary gate for our collected data. $CD3^+$ (T cells) and $CD19^+$ (B cells) (Figure S2F) were selected to evaluate the T and B cell counts in the lungs (Figures 2B and 2C). Our results revealed an increase in the numbers of T cells (Figure 2C) and B cells (Figure 2B) in the RB50Δ*btrS*-infected lungs at 7 dpi compared with RB50-infected lungs. When looking at ΔdblGATA-1 mice, the RB50Δ*btrS*-infected mice failed to increase the number of T and B cells recruited to the lungs, and the differences in T and B cells numbers between the two different infectious agents were absent. We also observed an increase in $CD4^+$ and $CD8^+$ cells that were exclusive to the BALB/c RB50Δ*btrS*-infected group, as suggested previously by the bulk transcriptomics data (Figure S2G). Nearly identical results were obtained in our secondary model using C57BL/6J and eosinophil-deficient *EPX/MBP*$^{-/-}$ mice (Figures 2D, 2E, and S2G).

Overall, our transcriptomics and flow cytometry data combined indicate that the bacterial pathway regulated by *btrS* suppresses host T and B cell recruitment in an eosinophil-

dependent manner (Table 1), leading to an impaired immune response associated with a longer bacterial persistence in the lungs.

btrS suppresses Th17 mucosal responses in an eosinophil-dependent manner

Because Th17 responses are critical for clearance of *Bordetella* spp.[55] as well as for the generation of protective immunity,[58,59] we investigated the interplay of the *btrS* bacterial factor in the suppression of Th17 immunity and involvement of eosinophils during the enhancement of Th1/Th17 responses. We analyzed transcriptomics data, focusing on Th17 markers (Figure 2F). We observed a higher number of transcripts of Th17-related cytokines in the BALB/c group infected with RB50Δ*btrS* than in mice infected with RB50. However, in the eosinophil-deficient ΔdblGATA-1 mice, these differences were ablated, with overall transcript numbers significantly reduced. These differences were further confirmed on our secondary eosinophil-deficient murine model using qRT-PCR (Figure S2E).

Next, we assessed secretome signatures in BALB/c wild-type mouse immune responses after challenge with RB50 or RB50Δ*btrS*. We isolated lung T cells on day 7 post infection using negative $CD3^+$ selection beads. Then, we stimulated them with CD3/CD28 beads for 48 h and performed an unbiased, blinded secretome analysis using the Isoplexis platform (Figures 2G-2I and S3A). In accordance with our transcriptomics analysis, we found higher levels of granulocyte-monocyte colony-stimulating factor (GM-CSF) (Figures 2G and S3A), IL-17 (Figures 2H and S3A), IFN-γ (Figures 2I and S3A), and IL-2 (Figure S3A) after infection with RB50Δ*btrS* compared with RB50, suggesting that wild-type *B. bronchiseptica* suppresses pro-inflammatory T cell responses via a *btrS*-mediated mechanism.

We next studied lung immune cells using intracellular flow cytometry to determine the numbers of $CD4^+$IFN-γ^+ and $CD4^+IL17^+$ T cells in the lungs of wild-type and eosinophil-deficient mice (Figures 2J and 2K). In contrast to BALB/c mice infected with RB50Δ*btrS*, whose $CD4^+$ cells secreted significantly higher levels of IFN-γ (Figure 2J) and IL-17 (Figure 2K), RB50 infected mice presented a reduced number of those cells. Eosinophil-deficient ΔdblGATA-1 mice revealed an impaired secretion of IFN-γ and IL-17, and the differences found between RB50- and RB50Δ*btrS*-infected groups disappeared in the ΔdblGATA-1 mice. Similar results were observed with *EPX/MBP*$^{-/-}$ mice (Figures 2L and 2M), suggesting that *B. bronchiseptica* uses *btrS* to block Th1/Th17 mucosal responses through an eosinophil-dependent mechanism (Table 1).

iBALT formation on day 7 post infection with a *btrS* mutant strain of *B. bronchiseptica*

Our transcriptomics analysis indicated that adhesion molecules such as GlyCAM (glycosylation-dependent cell adhesion molecule) or MadCAM-1 (mucosal vascular addressin cell adhesion molecule 1) and some chemokines, including CCL19, were highly increased exclusively in the wild-type mice challenged with the RB50Δ*btrS* strain (Figures 3A and S2E). These markers are associated with iBALT.[60,61] iBALT is known to form in the lungs as a response to multiple stimuli, such as infection with *P. aeruginosa*[62,63] or *K. pneumoniae*,[64] and it correlates with protection against reinfection.[64,65] iBALT is a tertiary lymphoid organ that consist of aggregates of lymphatic cells in peripheral areas of mucosal tissue.[63-65] Based on our previous results indicating rapid clearance[38] and protective

immunity[39] following infection with RB50Δ*btrS* combined with the transcriptomics, we hypothesized that RB50Δ*btrS* could promote early iBALT formation.

Lungs of BALB/c and ΔdblGATA-1 as well as C57BL/6J and *EPX/MBP*$^{-/-}$ mice challenged with RB50 or RB50Δ*btrS* were collected on day 7 post infection to perform H&E and immunofluorescence staining of paraffin-embedded, coded, blinded samples. The H&E staining revealed greater inflammation in the mice infected with RB50 in BALB/c and ΔdblGATA-1 mice. However, BALB/c mice challenged with RB50Δ*btrS* had numerous aggregates around the bronchiole area, as revealed by H&E staining (Figure S3B), following previously published classifications[64] (Figure S3C). Next, we performed immunofluorescence staining of specific B and T cells and other iBALT markers[66] (Figures 3B-3I). The results revealed that B and T cell numbers were low in the lungs of RB50-infected BALB/c mice, comparable with uninfected naive controls (Figures 3B-3G). Moreover, those cells were scattered throughout the lungs (Figures 3B and 3C). In contrast, in RB50Δ*btrS*-infected mice, B and T cell numbers were higher, and those cells formed aggregates characteristic of iBALT in both murine models (Figures 3B-3G). The aggregates were surrounded by endothelial hyaluronan receptor 1 (Lyve-1)-positive[67] lymphatic vessels (Figure 3I), and the less ubiquitous and highly germinal center-specific peripheral node addressin (PNAd)[68] (Figure 3H), distinctive features of iBALT. C57BL/6J mice showed similar results (Figures 3C, 3F, and 3G).

When we assessed responses in eosinophil-deficient mice, we found that the lungs of ΔdblGATA-1 mice infected with RB50 or RB50Δ*btrS* had lower numbers of B and T cells than uninfected controls (Figures 3B-3G), especially B cells. Similar results were obtained using the other eosinophil-deficient model, *EPX/MBP*$^{-/-}$ (Figures 3C, 3F, and 3G). It is important to note that iBALT was more prominent in BALB/c mice, where we also observed an increase in IL-5, in accordance with previously published data.[69]

The *btrS* gene regulates expression of the type 3 secretion system (T3SS), a well-known bacterial virulence factor,[70] so we investigated whether RB50 blocks iBALT through the T3SS. We inoculated groups of BALB/c and ΔdblGATA-1 mice with a functional mutant of the T3SS that lacks the ATPase that pumps effector proteins into the host cell but still expresses the apparatus machinery. Our results revealed that T3SS (RB50Δ*bscN*[71]) does not promote lung eosinophil recruitment (Figure S3D) or suppression of iBALT formation (Figure S3E). Although the T3SS undoubtedly contributes to the suppression of adaptive immune responses[72,73] and has a role in promoting persistence,[73] the observed blockage of eosinophil effector functions is caused by a *btrS*-regulated gene that remains to be elucidated. Altogether, our results suggest that *B. bronchiseptica* suppresses iBALT formation in a *btrS*-dependent manner (Table 1) and that eosinophils are required for iBALT formation.

Eosinophils promote mucosal responses in the lungs

We next wanted to investigate whether eosinophils might contribute to the increased Th1/Th17 responses observed in the lungs of RB50Δ*btrS*-infected mice and whether they promote an enhanced mucosal microenvironment within the iBALT. We challenged bone marrow-derived eosinophils[74] at a multiplicity of infection (MOI) of 10 with the RB50

or RB50Δ*btrS* strains. We performed an unbiased, blinded LegendPlex assay at 4 h post infection (Figure 4A). Eosinophils infected with RB50Δ*btrS* but not RB50 secreted significantly higher levels of IL-17a than the uninfected control, suggesting that eosinophils may contribute to pro-inflammatory responses.

Next, we took an *in vivo* approach where we sequentially immunostained blinded lung sections for $B220^+$ (B cells), MBP^+ (MBP contained in eosinophil granules) (Figures 4B and 4C), and IL-17a (Figures 4D and 4E). While eosinophils were less numerous and scattered in the lungs of RB50-infected mice, they were colocalized near B cells within the iBALT areas in mice challenged with RB50Δ*btrS* (Figures 4B and 4C). We observed an increase in the scattered IL-17a signal (Figures 4D and 4E) that did not colocalize with the iBALT in RB50-infected lungs compared with the uninfected mice. Conversely, in the mouse lungs infected with RB50Δ*btrS*, eosinophils were more abundant and colocalized in proximity to B cells in the iBALT and in surrounding areas. Thus, our results indicate that, without *btrS, B. bronchiseptica* infection promotes eosinophil recruitment within the iBALT, facilitating a Th17 microenvironment.

Another feature of strong mucosal responses is the increased concentration of immunoglobulin A (IgA). It has been shown previously that eosinophils promote IgA class switching,[75] and their correlation with increased levels of IgA at mucosal surfaces has been observed.[76] We performed immunohistochemistry of blinded coded lung sections using an anti-B220 monoclonal antibody combined with anti-mouse IgA (Figures 4F, 4G, S3F, and S3G). While uninfected mice and RB50-infected mice had very little IgA signal, mice challenged with RB50Δ*btrS* had a strong signal of IgA, specifically localized within the iBALT in the BALB/c and C57BL/6J models (Figures 4F, 4G, S3F, and S3G). Altogether, these data suggest that, during infection with a *btrS*-null *B. bronchiseptica* strain, eosinophils are recruited to the bronchiole area, where they colocalize with B cells, promoting mucosal immunity, including enhanced Th17 responses and IgA plasma cell formation, which possibly contributes to the early bacterial clearance.

Eosinophils are required for iBALT formation but not for its maintenance

It has been reported previously that eosinophils are required for mucosa-associated lymphoid tissue maintenance via secretion of APRIL (a proliferation-inducing ligand);[77] we wanted to investigate whether, in our model, eosinophils could serve a similar function in iBALT maintenance. We intranasally challenged BALB/c and ΔdblGATA-1 mice with PBS, RB50, or RB50Δ*btrS* and euthanized them on day 28 post infection. We collected the lungs to perform blinded immunostaining and assess iBALT. When analyzing BALB/c mice, our results revealed that the RB50-infected group had an increase in the numbers of B and T cells in the lungs, but no lymphoid aggregates were identified. Wild-type mice infected with the RB50Δ*btrS* strain maintained an organized and compact iBALT. Less inflammation was also noted (Figure 4H), perhaps because the mutant bacterial strain was cleared by day 28 post infection.[38] When examining the ΔdblGATA-1 mice, no iBALT was observed in any of the infectious groups, suggesting that, in the absence of eosinophils, iBALT is still not present on day 28 post infection when infected with either of the two bacterial strains.

Overall, these data indicate that, following infection with the RB50Δ*btrS* mutant strain, eosinophils are required for the initial iBALT formation and that, based on our data, they might not be required for its maintenance. However, because the latest time point included in our studies was day 28 post infection, we cannot assure that iBALT might not be present at later time points, independent of the action of eosinophils.

XCL1 is required for iBALT formation

We wanted to investigate the chemokines secreted by eosinophils in co-culture with both bacterial strains to identify possible chemokines that are related to iBALT establishment. Bone marrow-derived eosinophils[74] were challenged at an MOI of 10 with either bacterial strain, and a blinded LegendPlex chemokine assay was performed (Figure 5A). Eosinophils infected with the RB50 promoted increased secretion of XCL1, a chemokine involved in lymphocyte recruitment and enhanced antigen presentation. However, this increase was even more pronounced on eosinophils challenged with the RB50Δ*btrS*.

We then evaluated XCL1 levels *in vivo* by performing immunofluorescence staining to colocalize XCL1 and eosinophils (Figures 5B, 5C, and S3H). BALB/c mice infected with RB50 had only a slight increase in XCL1 (Figures 5B and 5C), and no colocalization was noted. Conversely, mice infected with RB50Δ*btrS* had higher levels of XCL1, and this was colocalized with eosinophils (Figures 5B and S3H). In ΔdblGATA-1 mice, the levels of XCL1 did not vary between the two infected groups and naive mice; the signal was also lower than expected, suggesting that, in eosinophil-deficient mice, the levels of XCL1 secretion were significantly impaired.

Given these results, we sought to evaluate the contributions of XCL1 to iBALT formation. We infected two groups of mice with the RB50Δ*btrS* strain. One group was left untreated, and the other group was treated daily intranasally with anti-XCL1 monoclonal antibodies (mAbs; 50 μg/mL in 15 μL).[78] On day 7 post infection, we collected the lungs and performed blinded immunostaining to evaluate iBALT formation. Our results showed that local treatment with anti-XCL1 mAb (50 μg/mL in 15 μL) can ablate iBALT formation (Figures 5D-5G and S3I). When measuring the levels of PNAd (Figure 5G), to further confirm the disruption of iBALT using a specific marker, our results indicate no changes in the PNAd levels compared with the shamchallenged group, further supporting that XCL1 promotes the formation of iBALT (Figure S3I). We then evaluated the use of 50 μg/mL in 30 μL of anti-XCL1 mAb to investigate whether increasing the volume would allow higher delivery into the lungs.[79] Indeed, our results reveal a higher effect in the suppression of B/T cell recruitment and subsequent iBALT formation (Figures 5D-5F). Thus, our results suggest that eosinophils potentially mediate iBALT formation via XCL1 secretion.

DISCUSSION

A commonality of bacterial pathogens is the need to overcome host immune responses and prevent the generation of mucosal protective immune responses.[80,81] We created a mutant strain of *B. bronchiseptica,* RB50Δ*btrS*, that cannot suppress host immune responses[38] and promotes the generation of long-lasting protective immune responses.[37] We have previously identified that eosinophils are critical in mediating immune responses to infection with this

mutant.[38] However, the specific role of these cells during adaptive immune responses to RB50Δ*btrS* were unclear.

Infection with *B. pertussis* and other respiratory pathogens, can facilitate the development of asthma and allergies.[49] However, the connection between both phenomena is not understood at a mechanistic level. It has been shown recently that SiglecF$^+$ neutrophils are critical for generating nasal Th17 protective immune responses during immunization against *B. pertussis*,[82,83] a granulocyte population typically associated with type 2 pathologies.[40] Eosinophils are critical during immune homeostasis[41] and lymphocyte-mediated responses.[46,77,84,85] Increased evidence of the role of these cells during bacterial infection is surfacing,[86,87] especially site-specific immune responses in the mucosal environment.[88] During *P. aeruginosa* infection, eosinophilia correlates with protection against infection.[89] Tracking eosinophil counts throughout disease progression has been proposed as a marker to evaluate antibiotherapy efficacy.[90] One question remains: why would bacteria target eosinophils to promote long-term persistent infections? Eosinophils not only have antibacterial activities themselves[89,91,92] but also play important roles during the establishment and maintenance of mucosal responses[41] and vaccine responses[46,93] because of their intrinsic relationship with lymphocytes[94-96] and the formation of lymphoid tissue during asthmatic pathologies[97] and its maintenance.[77] Because of their critical and important roles in homeostasis[41] and mucosal immune responses,[77,98] it is logical that bacteria target these cells to prevent the generation of robust immune responses and protective immunity, allowing persistence and reinfection.

Our results revealed that *B. bronchiseptica* delays the recruitment of T and B cells to the lungs on day 7 and suppresses the formation of iBALT through a *btrS*-mediated mechanism that targets eosinophils. It is undoubted that the T3SS plays an important role in immune suppression of *Bordetella* spp.[72,93,99] as well as in other species.[100,101] However, we believe that the suppression of the eosinophil effector functions is independent of the T3SS, and it might be caused by other *btrS*-regulated genes,[38] which we are currently investigating.

We identified an increase in the number of T cells recruited to the lungs in our RB50Δ*btrS* mutant that was dependent on eosinophils; notably, the increased total number and quality of T cells, which may explain[102,103] the long-lasting protective immunity.[39,103] Novel insights into *B. pertussis* epitopes found in humans revealed that there is a plethora of potentially new antigens to be explored,[104] and this *btrS*-null mutant strain may even expand the array of possibilities. We cannot overlook that there might also be an important role of CD8$^+$ T cells in this rapid clearance and protective immune response.[105] *B. bronchiseptica* suppresses B cell recruitment via a *btrS*-associated, eosinophil-dependent mechanism. In the absence of *btrS,* B and T cells form the iBALT, which is primarily formed by B cells that colocalize with eosinophils. Here, eosinophils can support B cell growth, proliferation, survival, and humoral responses,[106] including the production of antibodies.[96] In the absence of eosinophils, iBALT was not formed.

Our results revealed an increased Th17 response in mice infected with RB50Δ*btrS* that was ameliorated in the absence of eosinophils. Our previously published data revealed that infection with RB50Δ*btrS* leads to an enhanced Th17 immune response[38] and long-lasting

sterilizing immune responses in the lung.[39] A role of eosinophils and their ability to promote Th17 responses has been suggested previously based on cytokine profiles[40] and their immunomodulatory role.[107,108] Th17-eosinophil-mediated responses are involved in the autoimmune disorders observed in patients with hypereosinophilic syndrome[109,110] and during several infections, including *Aspergillus fumigatus*[111] or *Staphylococcus aureus*.[112] Based on our data, in the absence of *btrS* during *B. bronchiseptica* infection, eosinophils are required to promote Th1/Th17 responses, which are increased in the whole lung and accentuated in iBALT. Similarly, we observed increased IgA responses, suggesting a critical role of eosinophils in the formation of iBALT, which presents an enhanced mucosal response characterized by locally increased IL-17 and IgA levels. Eosinophils promote early establishment of iBALT via XCL1. These results reveal a novel role of eosinophils as promoters of pro-inflammatory mucosal responses against bacterial infections that was previously masked because of the bacterial ability to manipulate these cells as well as the lack of a clear model to understand the potential role of eosinophils.

It is important to highlight that our discoveries have occurred because we have a unique model that combines the wild-type bacteria that successfully block eosinophil effector functions and our *btrS*-null mutant. The findings presented here may draw parallels to other successful pathogens that may similarly suppress eosinophils, uncovering what may only be the beginning of novel possibilities in host-pathogen mucosal immunology.

We propose a model where *B. bronchiseptica* suppresses eosinophil effector functions through a *btrS*-mediated mechanism. When *btrS* is disrupted, eosinophils are recruited to the site of infection, where they promote B and T cell recruitment to the lungs and secretion of XCL1 to facilitate iBALT formation. A role of XCL1 in the generation of protective immunity has been indicated[113] in the context of viral infection. Our results uncover a new potential function of eosinophils as sources of XCL1 to enhance bacterial adaptive responses. When established, eosinophils mediate the formation of iBALT by promoting the expression of adhesion molecules, cytokines, and chemokines. Eosinophils colocalize within the iBALT, where they promote Th17 and IgA mucosal responses as well as survival and proliferation of B cells and IgA plasma cells (Table 1), altogether leading to robust, long-lasting protective immunity.[39] Moreover, the fact that we are unable to see a defect in clearance in eosinophil-deficient mice when infected with the wild-type bacteria further supports that the role of these cells is masked by an unknown mechanism that is mediated by *btrS* and that still remains to be elucidated in our future studies.

Conclusions

In this work, we unravel a new role of eosinophils during the generation of Th17 protective mucosal immunity against the respiratory pathogen *B. bronchiseptica.* Our results reveal that, during infection with wild-type *B. bronchiseptica,* eosinophils have no effect on infection dynamics in the lungs because of the ability of the bacteria to block their pro-inflammatory roles through a *btrS*-mediated immunosuppressive mechanism. However, when the bacterial sigma factor *btrS* is removed from the genetic background of *B. bronchiseptica,* eosinophils become critical for bacterial clearance from the lungs. During infection with this mutant, eosinophils promote B and T cell recruitment to the lungs

and mediate Th1/Th17 responses. Importantly, they also promote iBALT, which has an enhanced mucosal immune environment, possibly related to the characteristic long-term and protective immunity that this mutant provides against reinfection by any of the three classical *Bordetella* species, including the human pathogen *B. pertussis*. Overall, our results reveal a critical role of eosinophils during bacterial infection that has been long masked by the bacterial ability to manipulate these cells to allow persistence and subsequent reinfection.

Limitations of the study

Our study has some limitations that need to be disclosed. First, the current study is limited to *B. bronchiseptica*; we are investigating the remaining classical *Bordetella* species. Although we used two animal models, the use of a specific eosinophil Cre-knockout mouse model will be explored. Despite the high level of conservation of *btrS,* studies of this sigma factor in other bacteria are required to know whether *btrS* functions are conserved. The bacterial mechanism by which *B. bronchiseptica* suppresses eosinophil effector functions remains to be elucidated. Although our results suggest that the observed mechanisms are likely not T3SS mediated, in-depth studies are needed to fully unravel the molecular mechanism.

STAR★METHODS

RESOURCE AVAILABILITY

Lead contact—Further information and requests for resources and reagents should be directed to and will be fulfilled by the lead contact, Dr. Monica Cartelle Gestal (monica.cartellegestal@lsuhs.edu//mcarges@gmail.com).

Materials availability—This study did not generate new materials, reagents, mouse models, or plasmids.

Data and code availability

- RNA-seq data including the annotated version have been deposited at NCBI RefSeq and are publicly available. Accession numbers are listed in the key resources table. Microscopy and flow cytometry data reported in this paper will be shared by the lead contact upon request.
- This paper does not report original code.
- Any additional information required to reanalyze the data reported in this work paper is available from the lead contact upon request.

EXPERIMENTAL MODEL AND STUDY PARTICIPANT DETAILS

Bacterial strains—*B. bronchiseptica* strain RB50[36] (PMID: 8039908), a *btrS* knockout mutant[37,38] (PMID: 15130135; PMID: 31889098), and a *bscN* knockout[71] (PMID: 9663681) mutant generated in a previous study were used in this study.

Animal studies—For our animal experiments we used two complementary models of infant (Age = 8–24 weeks) mice[115,116] (PMID: 27307423; PMID: 32152071), one included

BALB/c and the eosinophil deficient pair, ΔdblGATA-1[54] (PMID: 9192642), mice originally purchased from Jackson laboratories, Bar Harbor, ME, and then bred in our facilities. GATA-1 mutation leads to complete ablation of the eosinophil lineage[52] (PMID: 12045237). Our secondary model included C57BL/6J purchased from Jackson laboratories and their eosinophil deficient pair, EPX/MBP$^{-/-}$ mice[53] (PMID: 28515227), that were kindly donated by Dr. Elizabeth Jacobsen at the Mayo Clinic. These mice have a mutation in the eosinophil peroxidase and the eosinophil major basic protein, leading to a specific removal of the eosinophil populations.

Our breeding colonies were kept under the care of the employees and veterinarians of the Animal Care Facility within Louisiana State University Health Sciences Center at Shreveport, LA., which is accredited by the Association for Assessment and Accreditation of Laboratory Animal Care (AAALAC). All experiments were carried out in accordance with all institutional guidelines (AUP:20–038, AUP:22–031). Our mice are bred in-house to avoid changes due to the microbiota of the mice. To maintain the genotypes of each mouse strain, each breeding colony is regenerated after 5 generations. All mice were maintained under a 12-h light/dark (7a.m.-7p.m.) cycle in pathogen-free conditions at all times under the care and maintenance of the institutional Animal Care Facilities.

The sex of any mouse strains used has no influence on, or association with, the results presented in this study.

METHOD DETAILS

Bacterial culture conditions—*B. bronchiseptica* RB50 and mutants were cultured in Difco Bordet- Gengou (BG, BD Biosciences, #248200) and supplemented with 10% sheep defibrinated blood (Hemostat, #DBB500) with 20 μg/mL streptomycin (Gibco, #11860-038) or classical LB broth (Fisher, #BP1425-500), Stainer-Scholte media[117] (PMID: 4324651), or Bordet-Gengou Agar as previously described[118] (PMID: 30245672).

Bacterial strain liquid inoculum—To prepare the inoculums we grew the bacteria overnight in Luria Bertani[118] (PMID: 30245672) or Stainer-Scholte media[117] (PMID: 4324651). The day after we measured the OD at 600 nm and the culture was diluted to an OD of 0.1 at 600nm. An OD_{600} = 0.1 corresponds with 10^8 CFU/mL of *Bordetella* spp.[38,118] (PMID: 30245672; PMID: 31889098). A series of 100-fold dilutions (10^8–10^2 CFU/mL) were prepared to obtain $10^{6–7}$ CFU/mL which was used to inoculate 15–25 mL of inoculum per nostril. The remaining serial dilutions (10^4 and 10^2 CFU/mL) from the prepared inoculum were plated to enumerate bacteria contained in the inoculums.

Bacterial inoculation mouse procedure—Briefly, for our animal inoculations, mice were anesthetized with 3–5% volume-to-volume (v/v) isoflurane (Attane, #RXISO-250) and when asleep (relaxed breathing rate) they were intranasally challenged with 30-50μL of PBS (Gibco, #10010-031) containing 5x10^5 CFU/mL *B. bronchiseptica* RB50, RB50Δ*bscN*, and RB50Δ*btrS*. Monitor the respiratory rate of the mice while undergoing this procedure and begin inoculations when their breathing slows to ~55–65 breaths per minute (PMID: 34180990). To take additional precaution about the anesthetic state, ensure there is no major

corneal reflex (blinking when touched) or limb reflexes by pinching the paws and tail periodically before proceeding (Anesthesia stages. Siddiqui, 2023. *StatPearls*).

For the inoculations, we delivered half of the inoculum in each nostril. After inoculation, animals were deposited back on their cages on their back and monitored for 5 min as established in our animal protocols prior to deliver back in the procedure room. Euthanasia was performed if humane endpoints were reached prior to the end of the experiment.

Animal procedures

Euthanasia: To perform the organ collection, 2mL reinforced homogenizer tubes (VWR, #10158-556) containing a mixture of 0.5 mm and 1.4 mm ceramic beads were used. Before use, the collection tubes were autoclaved using the vacuum sterilization cycle at 121 °C (250°F) for 20–30 min at 15 psi before the addition of phosphate-buffered saline (PBS). For rigor and reproducibility, all experiments were blinded using a de-identification coding system, so the tubes were labeled accordingly with the appropriate code. After each analysis, the results were unblinded and associated with a mouse, genotype, gender, and age using our coding database.

Once in the animal procedure room, mice were placed on a chamber where the CO_2 flow rate was displaced at 10–30% volume-to-volume of cage per minute (Guidelines for Euthanasia of Rodents Using Carbon Dioxide). When the mice do not present any thoracic movement (i.e., respiratory arrest), confirm heavy sedation of the mouse by testing absence of corneal reflexes (i.e., no blinking when the inner eye is touched) or limb reflexes by pinching the paws or tail. Upon sufficient anesthetization, we then proceed with cervical dislocation and tissue collection.

Organ collection to perform colonization studies: Briefly, to perform the organ collection we used 2mL reinforced homogenizer tubes (VWR, #10158-556), containing 1mL of cell-grade culture sterile PBS and a mixture of 0.5 mm and 1.4 mm ceramic beads (PMID: 37065208). After organ collection in the animal room, we used the Bead Mill Homogenizer (VWR, 75840-022) and used the cycle with a speed = 2.75 m/s, rotary distance of 0.03, 5 combined cycles of 1:30 min runs, and total run time of 7.5 min. After the cycle, the dissociated tissue is spread onto plates containing Bordet-Gengou agar supplemented with 1:100 dilution of streptomycin (20 mg/ml) using serial 100-fold dilutions (0, −2, −4).The spread plates are then incubated for 36–48 h at 37°C in 5% CO_2. A CFU a range between 20 and 200 CFU/mL is considered countable. For the data analysis, the average of all CFU counts regardless of dilution factor was counted to plot and visualized using GraphPad (see more in the statistics section).

Perfusion and organ collection to perform pathological studies—Pathology experiments were performed in at least 2 independent inoculations, containing at least 4 mice per time point and infectious group. The total number of mice was ≥6 for all the experiments done in BALB/c and ΔdblGATA-1; and at least 4 for all the experiments performed with C57BL/6J and EPX/MBP$^{-/-}$ mice. For all pathology experiments, mice were euthanized and intratracheally perfused with sterile PBS and 4% paraformaldehyde[119] (PFA, Electron microscopy sciences, Cat #19210; PMID: 32831298). Lungs were

subsequently fixed overnight in 10 mL of 4% PFA. After 48 h, the PFA was replaced by 70% ethanol and the samples were delivered to the Animal Models & Histology core of the COBRE Center for Redox Biology and Cardiovascular Disease, funded by the National Institutes of Health (NIGMS P20 GM121307). Lungs were processed, paraffin-embedded, sectioned into 0.5 μm thick slices, then placed on glass slides by the COBRE Histology Core at LSU Health Shreveport, LA. All microscopic analyses were performed in 2-3 sections per mouse and at least 10 areas were collected for each section. All slides were blinded using a coding system which was revealed only after the staining, evaluation, imaging acquisition and analysis was completed.

Organ collection to perform transcriptomic analysis—After euthanasia, a quarter of a lung was collected in a 2mL reinforced homogenizer tube (VWR, #10158-556), containing 1mL of Trizol[120] (PMID: 33815807) and a mixture of 0.5 mm and 1.4 mm glass and ceramic beads (PMID: 37065208). For extraction of the whole lung, 4 tubes were used each containing a quarter of a lung. After homogenizing in the Bead Mill Homogenizer (VWR, 75840-022) and proceed with the following cycle, S = 2.75 m/s, 5 cycles of 1:30 min runs, distance 0.03 and total run time of 7.30 min, we proceed to we continue with the RNA extraction method (see description below).

Anti-XCL1 treatment—Briefly, following infection with the RB50Δ*btrS* strain, mice were intranasally inoculated with 15–30 μL of 50μg/ml anti-XCL1 (Leinco, #L229) every day[78] (PMID: 32849609), starting at day 1 post-infection. Treatment was delivered every day at the same time within an interval of 30 min. After mice were anesthetized, we intranasally delivered the antibody, half of the volume in each nostril. Treatment was daily up to day 7 post-infection coinciding with the end of the experiment.

RNA extraction—For RNA extraction[38,118] (PMID: 30245672; PMID: 31889098) of mouse tissue, we added 1 mL of Trizol (Ambion, #15596018) into beaded tubes and collected one-quarter of the lung per tube. If the whole lung RNA was to be extracted, extraction was performed, and lung tissue was evenly distributed amongst 4 separate tubes and combined into a single tube following elution. To perform the extraction, we started by washing the Trizol with chloroform. Then, we proceeded with the protocol provided by the manufacturer (PureLink RNA Extraction Kit, Invitrogen Cat #2365053). We followed the high-quality extraction protocol which included a treatment with RNAse (PureLink DNAse Kit, Invitrogen Cat #12185010). Elution was performed in RNAse-free water. Quantification was done by using the NanoDrop One-C (Cat #A241601534). We ensured that the A230:260:280 ratio was approximately 1:2:1. After quantification, RNA was stored at −20°C until use.

Bulk lung RNA sequencing—At day 7 post-inoculation, mice were euthanized according with humane endpoints and our protocol approval. Lungs were collected in 4 different beads tubes containing Trizol (Ambion, Cat #15596018) and kept on ice for the shortest time possible before being homogenized and frozen at −20°C. For RNA extraction, we used RNAseZap (Invitrogen, Cat #AM9780) and followed the protocols recommended by the manufacturer, PureLink RNA Extraction kit (Invitrogen, Cat #2365053). The 4

different tubes, containing quarters of the lung, were pooled back together at the end of the extraction to have the whole lung RNA represented in one only preparation. We used 3–4 naive animals and between 5 and 6 infected mice for each condition.

Twenty-four total RNA samples were assessed and processed for sequencing. For lung RNA sequencing, samples were delivered to our Modeling Core, of the COBRE Center for Applied Immunology and Pathological Processes at LSU Health Science at Shreveport. Sequencing report (attached in supplementary material) includes all the detail of the sequencing. Samples were quantitated with a Qubit RNA assay (ThermoFisher Scientific) and RNA quality was determined with the Agilent TapeStation RNA assay (Agilent Technologies). Libraries were prepared with the Stranded mRNA Prep, Ligation kit (Illumina). One mg of RNA was processed for each sample: mRNA was purified and fragmented. cDNA was synthesized, and 3′ ends were adenylated. Anchor sequences were ligated to each sample and limited-cycle PCR was performed to amplify and index the libraries. The average library size (330–355) was determined using an Agilent TapeStation D-1000 assay (Agilent Technologies) and libraries were quantitated with qPCR (Bio-Rad CFX96 Touch Real-Time PCR; NEB Library Quant Kit for Illumina). Libraries were normalized to 0.5 nM and pooled. The library pool was denatured and diluted to approximately 100 p.m. A library of 2.5 p.m. PhiX was spiked in as an internal control. Paired end 75-cycle sequencing was performed on an Illumina NovaSeq 6000 (Supplementary Report and key resources table). Accession number: E-MTAB-13332.

qRT-PCR—RNA concentration was adjusted to 1 mg/ml with RNAse-free water. Results obtained by RNA-Seq were further confirmed using qRT-PCR following the recommendations of the manufacturer, Luna One-Step qRT-PCR (New England Biolabs, #E3005X). The primers used for each specific gene of interest were previously published (key resources table). qRT-PCR was performed in the CFX96 Bio-Rad. Negative controls and non-template controls were used in each qRT-PCR to exclude possible contaminations. Analysis of the results to obtain $\Delta\Delta C_q$ values was calculated after normalization with actin and following the instructions provided in the Luna One-Step qRT-PCR kit as well as previously published protocols. All qRT-PCR were performed with at least 4 different animals, in three technical replicates each time and in our both independent animal models previously explained. The amounts of reagent per reaction were as follows.

Table:

Concentrations of reagents required for the qRT-PCR

PCR (reaction: 20 µL)	
Reagent	Final reaction concentration
Luna Universal One-Step Reaction Mix (2X)	1X
Luna WamSmart RT Enzyme Mix (20X)	1X
Forward Primer (10 mM)	10 µM
Reverse Primer (10 mM)	10 µM
Template RNA (≤1 µg)	<1µg
Nuclease-free water	To 20 µL

Flow cytometry

GentleMacs and single cell preparation **(Miltenyi Biotech, #130-095-927):** Following euthanasia, we collected the lungs in tissue dissociation tubes (Miltenyi Biotech, Cat #130-093-237) after cutting them into quarters. The dissociation tubes contained the lung dissociation solution (Miltenyi Biotech, Cat #130-095-927). These tubes were put on the GentleMacs upside down and fasten in the apparatus. We added the heater (tightly fastened), then started the GentleMACS cycle (37C_m_LDK_1) that corresponded with the 30 min lung dissociation cycle.

After the cycle ended, we followed the standard procedures. Briefly, we washed twice with DPBS and then treated them with ACK lysis buffer (Gibco, Cat #A1049201) for 5 min at room temperature and proceeded with centrifugation. After discarding the supernatant, we resuspended the pellet in complete RPMI (Gibco, Cat #11875119), supplemented with 10% fetal bovine serum (FBS, Gibco, Cat #10437028) and 50 μM β-mercaptoethanol (Sigma, Cat #60-24-2] and filtered the cell suspension with a 40 μm filter (Cat # 352340 Falcon). We then counted the cells in the Countess-III Cell Counter (ThermoFisher, #AMQAX2000).

Staining for flow cytometry and analysis—To stain for intracellular cytokines, cells were seeded in the 96 well V-bottom plate ($2x10^6$ per well) and were stimulated for 4–5 h with the cell stimulation cocktail containing brefeldin A (BioLegend, Cat #423303) at 37°C. After stimulation, we proceeded with cell staining following the standard flow cytometry staining procedures[38,40,121] (PMID: 31889098; PMID: 31633216). Briefly, cells were washed with DPBS (Corning, Cat #21-031-CV) and first stained with Zombie Yellow fixable viability dye for 30 min at room temperature to exclude the dead cells. Fc receptors were then blocked by incubating cells in TruStain Fcx plus Fc block (BioLegend, Cat #156604) in FACS buffer (DPBS containing 2% FBS and 2mM EDTA) at 4°C for 10 min. The surface staining was performed for 30 min at 4°C using anti-mouse antibodies against CD45 (30-F11), CD3 (17A2), CD4 (GK1.5), CD8 (53–6.7), CD19 (6D5), CD11b (M1/70), Ly6G (1A8) and SiglecF (S17007L), all from BioLegend. Following surface staining, cells were fixed and permeabilized with eBioscience Foxp3 fixation/permeabilization staining kit (Invitrogen, #00-5523-00) according to the recommended protocol. Intracellular staining was done in 1X permeabilization buffer for 1 h at 4°C using anti-mouse antibodies against IFN-γ (XMG1.2), IL-5 (TRFK5) and IL-17A (TC11-18H10.1). After intracellular staining, cells were washed twice with 1x permeabilization buffer and once with FACS buffer. Single-color, unstained, and fluorescence minus one control (FMOs) were prepared for each staining experiment.

Table:

Antibodies used for flow cytometry in this paper

Antibody/Reagents	Conjugate	Clone	Source	Catalog	Dilution
Zombie Yellow Fixable Viability dye	N/A	N/A	BioLegend	423103	1:500
TruStain FcX plus (anti-mouse CD16/32) antibody	N/A	S17011E	BioLegend	156604	1:200
Rat anti-mouse CD45	BV510	30-F11	BioLegend	103138	1:400

Antibody/Reagents	Conjugate	Clone	Source	Catalog	Dilution
Rat anti-mouse CD3	BV711	17A2	BioLegend	100241	1:100
Rat anti-mouse CD19	AF700	6D5	BioLegend	115528	1:800
Rat anti-mouse CD4	BV785	GK1.5	BioLegend	100453	1:400
Rat anti-mouse CD8a	AF488	53–6.7	BioLegend	100723	1:400
Rat anti-mouse INF-y	PE/Cy7	XMG1.2	BioLegend	505825	1:100
Rat anti-mouse/human IL-5	APC	TRFK5	BioLegend	504305	1:50
Rat anti-mouse IL-9	BV421	RM9A4	BioLegend	514109	1:200
Rat anti-mouse IL-13	PE-eFluor610	eBio13A	ThermoFisher	61-7133-82	1:50
Rat anti-mouse IL-17A	PerCP/Cy5.5	TC11-18H10.1	BioLegend	506920	1:100
Rat anti-mouse IL-33	PE	396118	ThermoFisher	MA5-23640	1:10

Histology: Immunostaining—To perform our immune staining, we followed protocols previously published by our collaborators[122] (PMID:37223953). Briefly, slides with PFA fixed and paraffin-embedded tissues were de-paraffinized in consecutive washes in xylene (Azer Scientific, Cat #E5609), followed by re-hydration, PBST washes, and citrate buffer solution for antigen retrieval. Antigen retrieval wash was done by steaming slides in a citrate buffer with a pre-heated Instant Pot pressure cooker for 10 min at medium heat. After cooling down and washes, PBS supplemented with 0.2% Triton X-100 (VWR, Cat #9002-93-1) was used to permeabilize the tissues. After blocking for 90 min in 13 mL of 0.15% Bovine Serum Albumin (BSA, Fisher, Cat #BP9703-100) with Normal Goat Serum (Vector, Cat #S-1000) and PBST, slides underwent PBST washes prior to staining. Staining was performed using the appropriate primary antibodies diluted with 0.15% BSA in PBST (see the table in the “Staining for flow cytometry and analysis” section) and incubated overnight. The next day, secondary antibodies were used prior to Hoechst 33342 (BD Biosciences, Cat #561908) staining. Slides coverslips were mounted to the sections with ProLong Glass Antifade Mountant (Invitrogen, Cat #P36984) and dried in the dark at room temperature until later analysis.

Eosinophils *in vitro*—BALB/c mice were euthanized accordingly with our IACUC protocol guidelines. We cleaned the femur and tibia. We flashed the inside of the bones with RPMI to obtain Bone marrow progenitors. To differentiate them into eosinophils we followed previously published protocols[74] (PMID: 33486726). Briefly, Single cell suspensions of bone marrow progenitors were incubated in eosinophils base media containing 100 ng/ml rmFLT3L (PrepoTech, #250-31L) and 100 ng/mL rmSCF (PrepoTech, #250-03) for 4 days. The cells were then maintained in eosinophil base media supplemented with 10 ng/mL IL-5 (PrepoTech, Cat #215-15) for up to 16 days. Percentage of differentiation was evaluated by flow cytometry and/or cytochemical staining[74] (PMID: 33486726).

Infection of eosinophils *in vitro*—For the infection, multiplicity of infection (MOI) was calculated in function of the number of eosinophils per well. Confluency was not considered, as eosinophils do not attach. MOI = 0.1, 1, and 10 were used on our assays as indicated in each figure. Bacteria were then resuspended in eosinophils base media to

perform the infections. After adding bacteria, the plates were spun down at 300 x g for 5 min. All assays were performed in at least 3 independent biological replicates, containing 6 technical replicates each time. The supernatant of the *in vitro* infections was collected at 4 h post-infection and kept at −20°C until ready for use.

Amino acid multiple sequence alignment and functional domain analysis—An NCBI Protein BLAST (pBLAST) search was performed using the amino acid sequence of the *btrS* gene from *Bordetella bronchiseptica* RB50 (NCBI Accession: WP_003809919.1, UniProt ID: A0A0H3LK62_BORBR). The FASTA files containing *btrS*-like amino acid sequences were exported and aligned using the Clustal Omega Multiple Sequence Alignment (MSA) viewer. The Clustal Alignment Format (.aln) file was uploaded and visualized using the Jalview software (https://www.jalview.org/) for customization and addition of annotations of the aligned amino acid sequences. Sequence domain annotations were retrieved from the PANTHER domain database (https://www.pantherdb.org/panther/family.do?clsAccession=PTHR43133), under the ECF RNA polymerase sigma factor domain family (PANTHER Accession: PTHR43133) for functional homology analysis. Intensity of residue color corresponds to an increasing score with combined factors of percent identity (PID), total alignment conservation, and alignment quality based on Blosum62 substitution matrix score through the analysis provided by the Jalview desktop software. A consensus amino acid sequence was also generated using Jalview and can be seen below the multiple amino acid sequence alignment.

QUANTIFICATION AND STATISTICAL ANALYSIS

Statistical analysis—All experiments were performed in three independent biological replicates. The exact number of mice and technical replicates and the test performed is indicated in each figure legend. Statistical tests were applied based on previous literature[123,124] (PMID: 31274493; PMID: 12391400). For animal experiments we performed two-way ANOVA analysis, while qRT-PCR experiments were analyzed using One-way ANOVA analysis. Similarly, all the data that was normally distributed was analyzed using One-way and two-way ANOVA test as indicated in each figure legend. When ANOVA was not an option, Student's T tests were performed. All graphs and data were analyzed using the GraphPad (v10.0.2). A p value ≤ 0.01 was considered statistically significant. In the figures, the asterisks correspond with *$p \leq 0.01$, **$p \leq 0.005$, ***$p \leq 0.001$, and ****$p \leq 0.0001$.

Statistical analysis for sample size—To assure that a correct sample size[125] (PMID: 24250214) was used that resulted in statistical power we utilized the Russ Lenth's power[126] (PMID: 17060421) calculator to estimate the number of mice needed per group to obtain a power of 80% and considering at least a 20% standard deviation. All animal experiments were done in at least two independent times containing at least 4–5 mice per group each time. All studies were done in male and female infant mice to be able to detect gender specific responses if those were detected that it was not the case in our studies. In each figure the number of mice is indicated as "n", followed by the statistical test used in each individual analysis.

Quantification

Flow cytometric analysis: Cells were acquired on our NovoCyte Quanteon flow cytometer (Agilent, CA), and data was analyzed with FlowJo software v10.9 (TreeStar, Ashland, OR). Gating strategy is shown in supplementary material (Figure S2G). All immunology experiments were performed at the Immunophenotyping Core, of the COBRE Center for Applied Immunology and Pathological Processes at LSU Health Shreveport, LA.

To obtain total cell numbers from the flow cytometry results, we consolidated the percentages with the total number of cells by using the following calculation: (% frequencies) x (total number of cells) x (0.01)[38,40] (PMID: 31889098). Results were graphed in GraphPad (see details for the analysis below).

LegendPlex analysis—For the assay, the recommendations for LegendPlex were closely followed per BioLegend. We used the Thelper v13 (BioLegend, #741044) and chemokines (BioLegend, #740451). At least 4 independent biological replicates (all in technical duplicates as indicated in each figure legend) were performed. For analysis, the cloud software recommended by BioLegend (legenplex.qognit) was used. All, the protocol and analysis, were done following the manufacturer recommendations.

Microscopy image acquisition and analysis—For analysis with the Keyence Image Analysis Software (v1.1.2) of each immunofluorescence assay a fluorescence intensity threshold was set and used to detect Hoechst stain lung cells that were also positive for each target antibody. This was done under the double extraction section of the software. Where the first step was to set the threshold for the antibody target and the second step was to set the threshold for the nuclear stain. Each group of images analyzed in this manner was done in batch analysis using the same threshold settings. We performed staining of three independent sections of 6 different BALB/c mice per group (infected at different times) and acquired at least 10 different images per section of each animal.

Colocalization analysis of XCL1 with MBP was done using the Imaris 3D analysis software v10[127] (PMID: 36672153). This was done using the intensity base colocalization future of the software. For this, a standard threshold intensity was set for both the channel showing the MBP expression and the channel showing the XCL1 expression. The colocalized intensities were then masked into a separate channel overlaying the image to show colocalization. The quantitative results, including the Pearson Coefficient, Manders Coefficient, number of overlapped voxels, and percentage of area colocalized were given in an output excel file for each image analyzed. From these outputs, the percentage of area colocalized from each image was plotted and statistically analyzed using GraphPad Prism (v10.0.2).

Immunofluorescent images of the lungs were captured using a Keyence BZX-800 microscope. Image analysis was conducted using the Keyence Image Analysis Software. Briefly, for analysis of each immunofluorescence assay a fluorescence intensity threshold was set and used to detect Hoechst stain lung cells that were also positive for each target antibody. Each group of images analyzed in this manner was done in batch analysis using the same threshold settings. We performed staining of three independent sections of 6

different BALB/c mice per group (infected at different times) and acquired at least 10 different images per section per animal. Complete list of antibodies is included in the key resources table.

IsoPlexis analysis—Following inoculation with RB50 or RB50Δ*btrS*, groups of 4 mice were euthanized. Lungs were collected in 5 mL of cold PBS and were kept on ice. To obtain single cell suspensions, mouse lung dissociation kit (Miltenyi Biotec, Cat #130-095-927) was used, and the dissociation was carried out using GentleMacs Octo-Dissociator (Miltenyi Biotec). T cells were isolated from the above-mentioned single cell suspensions using the MojoSort Mouse CD3 T cell Isolation Kit (BioLegend, #480024). 10^6 T cells per well were then seeded in a 96-well U-bottom plate in a volume of 200 μL with complete RPMI. To activate T cells, 25 μL of Mouse T-Activator CD3/CD28 Dynabeads (Invitrogen, #11452D) was added to the wells and cells were incubated at 37°C and 5% CO_2 for 48 h. Following incubation, cell culture supernatant was harvested by spinning down the samples at 5000 rpm for 10 min at 4°C. CodePlex chip (CodePlex Inflammation-L Chip 2, #CODEPLEX-2L-10-2) was thawed for 1 h at room temperature. Using a P-10 pipette, 5.5 μL of each sample was loaded into each MacroChamber of CodePlex Proteomic Barcoded Chip. The chip and CodePlex liquid reagent was then loaded into an IsoSpark automation system (PhenomeX, CA) and various proteins were measured by fluorescence ELISA and analyzed by the IsoSpeak software using the IsoPlexis Mouse Adaptive Immune Panel: GM-CSF, IFN-γ, IL-1β, IL-2, IL-4, IL-5, IL-6, IL-10, IL-12, IL-17A, IP-10, KC, MCP-1, MIP-1α, RANTES, and TNF-α. All immunology experiments were performed at the Immunophenotyping Core of the COBRE Center for Applied Immunology and Pathological Processes at LSU Health Shreveport.

RNA analysis—Our Illumina FASTQ files were shared with our collaborators at the supercomputational center of Galicia (CESGA) to perform the analysis with our collaborators. Adaptors and low-quality bases were removed using Trimmomatic (version 0.38). Index was generated using Rsem software (version 1.3.1) utilizing *Mus musculus* reference genome version GRCm39and gene transfer format (.gtf) annotation version GRCm39.105 (NCBI RefSeq Assembly Number: GCF_000001635.23) from Ensembl. Reads were aligned using STAR (version 2.7) and expression values were calculated using Rsem (version 1.3.1). Differential gene expression was evaluated using DESeq2 R package (version 1.34.0). Benjamini-Hochberg correction was used to obtain adjusted p values. Shrunken $\log_2$ fold changes were obtained using 'ashr' shrunkage. Genes with adjusted p value <0.05 and absolute $\log_2$ fold-change ≥ 1.5 were considered significant in terms of differential expression. Gene Set Enrichment Analysis (GSEA) and over-representation (OR) test for differentially expressed genes were performed using Clusterprofiler (version 4.2.2) and Gene Ontology – Biological Process collection for mouse. Benjamini-Hochberg correction was used to obtain adjusted p values. Redundant terms in over-representation analysis were reduced using the simplify function, with a cutoff value = 0.6.

Analysis of fold-change expression of qRT-PCR—Briefly, after the qRT-PCR ended in our Bio-Rad CFX96 qRT-PCR, data was collected as an excel document that included all the information of the run and the raw data. We then designed an excel template to input that

data and obtain the fold change values. Our calculations[128] (PMID: 30654913) are detailed below.

1. To find the ΔC_q value:
   a. Extract the C_q values of each sample from the qRT-PCR data.
   b. Calculate the average control C_q value for each target sample.
2. Find the difference between the average ΔC_q control values and the C_q value of the target gene. This is the ΔC_q value.
3. Next, find the average of the mean C_q control values previously calculated. This is the "Average Control" value, and it should only be one number. You will reference back to the number to calculate the relative gene expression (fold-change expression) in the next step.
4. To calculate the $\Delta\Delta C_q$ value, find the difference between the ΔC_q value of the desired sample and the "Average Control" from (3). Do this for each unknown C_q value (i.e., each unknown sample).
5. Calculate the $2^{-\Delta\Delta Cq}$ value from each $\Delta\Delta C_q$ value to determine the relative fold-change gene expression of each sample that is relative to the control target genes.

Rigor and reproducibility

- All experiments were performed in at least 2–3 independent biological replicates including at least 3 technical replicated. All our experiments are logged in folders containing our standard operational procedure (SOP) and protocols, including specific notes for each individual experiment. *In vitro* samples were blinded for the multiplex Elisa assay and its analysis.
- All mice samples were enumerated using a blinded coding system and divided into groups based on mouse strain and inoculum. Results were unblinded following each analysis using our animal database that contains all appropriate mouse information (i.e., genotyping, date of birth, gender, etc.) and experimental information (i.e., inoculum, dosage, day post-infection experimental protocol, etc.). All animal experiments were performed following the laboratory standard operational procedures and each logged experiment is recorded, collected, and stored for tracking of all animal procedure cards and experimental information.

Supplementary Material

Refer to Web version on PubMed Central for supplementary material.

ACKNOWLEDGMENTS

We would like to acknowledge the support of the funding bodies, which had no role in the study design, data collection, data analysis, or data interpretation: NIH COBRE award P20-GM134974, Louisiana Board of Regents LEQSF(2022-25)-RD-A-33, Center of Excellence for Arthritis and Rheumatology intramural award, and Intramural Research Council Seed and Start-up package from LSU Health, Shreveport. The genomic analysis was partially supported by Xunta de Galicia (Grupo de Referencia Competitiva, ED431C 2020/02). A.M.-P. acknowledges a

fellowship from Xunta de Galicia (Programa de Axudas á etapa predoutoral, Consellería de Cultura, Educación e Ordenación Universitaria, ED481A-2018/230). We also thank the Galician Supercomputational Center (CESGA), whose services allowed the bioinformatics analysis. We want to acknowledge the centers funded by our COBRE P20-GM134974, the immunophenotyping core, and the Bioinformatics and Modeling Core. We acknowledge the Animal Models & Histology core of the COBRE Center for Redox Biology and Cardiovascular Disease, NIGMS P20 GM121307, for histology and pathology support. We would also like to acknowledge Martin Sapp for his ideas, brainstorming, and support during editing. We would like to thank the Undergraduate Biomedical Research Fellowship Program at the Department of Microbiology and Immunology, which supported Emily Cox, and the Summer Undergraduate Research Fellowship Program of the Fundación Barrie de la Maza and LSU Health Shreveport, which supported Jose Pedreira-López and Laura López-Candales.

INCLUSION AND DIVERSITY

We support inclusive, diverse, and equitable conduct of research. One or more of the authors of this paper self-identifies as an underrepresented ethnic minority in their field of research or within their geographical location. One or more of the authors of this paper received support from a program designed to increase minority representation in their field of research.

REFERENCES

1. Baker RE, Mahmud AS, Miller IF, Rajeev M, Rasambainarivo F, Rice BL, Takahashi S, Tatem AJ, Wagner CE, Wang LF, et al. (2022). Infectious disease in an era of global change. Nat. Rev. Microbiol 20, 193–205. 10.1038/s41579-021-00639-z. [PubMed: 34646006]
2. Pollard AJ, and Bijker EM (2021). A guide to vaccinology: from basic principles to new developments. Nat. Rev. Immunol 21, 83–100. 10.1038/s41577-020-00479-7. [PubMed: 33353987]
3. Slim MA, van Mourik N, Dionne JC, Oczkowski SJW, Netea MG, Pickkers P, Giamarellos-Bourboulis EJ, Müller MCA, van der Poll T, Wiersinga WJ, et al. (2022). Personalised immunotherapy in sepsis: a scoping review protocol. BMJ Open 12, e060411. 10.1136/bmjopen-2021-060411.
4. Wadman M, and You J (2017). The vaccine wars. Science 356, 364–365. 10.1126/science.356.6336.364. [PubMed: 28450592]
5. Bouchez V, Guillot S, Landier A, Armatys N, Matczak S, Toubiana J, Brisse S, and group F.p.m.s. (2021). Evolution of Bordetella pertussis over a 23-year period in France, 1996 to 2018. Euro Surveill. 26. 10.2807/1560-7917.ES.2021.26.37.2001213.
6. Melvin JA, Scheller EV, Miller JF, and Cotter PA (2014). *Bordetella pertussis* pathogenesis: current and future challenges. Nat. Rev. Microbiol 12, 274–288. 10.1038/nrmicro3235. [PubMed: 24608338]
7. Mattoo S, and Cherry JD (2005). Molecular pathogenesis, epidemiology, and clinical manifestations of respiratory infections due to *Bordetella pertussis* and other *Bordetella* subspecies. Clin. Microbiol. Rev 18, 326–382. 10.1128/CMR.18.2.326-382.2005. [PubMed: 15831828]
8. Macina D, and Evans KE (2021). *Bordetella pertussis* in School-Age Children, Adolescents, and Adults: A Systematic Review of Epidemiology, Burden, and Mortality in the Middle East. Infect. Dis. Ther 10, 719–738. 10.1007/s40121-021-00440-8. [PubMed: 33905101]
9. Muloiwa R, Nicol MP, Hussey GD, and Zar HJ (2020). Diagnostic limitations of clinical case definitions of pertussis in infants and children with severe lower respiratory tract infection. PLoS One 15, e0235703. 10.1371/journal.pone.0235703. [PubMed: 32678857]
10. Karalius VP, Rucinski SL, Mandrekar JN, and Patel R (2017). *Bordetella parapertussis* outbreak in Southeastern Minnesota and the United States, 2014. Medicine (Baltim.) 96, e6730. 10.1097/MD.0000000000006730.
11. Liu X, Wang Z, Zhang J, Li F, Luan Y, Li H, Li Y, and He Q (2018). Pertussis Outbreak in a Primary School in China: Infection and Transmission of the Macrolide-Resistant Bordetella pertussis. Pediatr. Infect. Dis. J 37, e145–e148. 10.1097/INF.0000000000001814. [PubMed: 29088029]

12. Wensley A, Hughes GJ, Campbell H, Amirthalingam G, Andrews N, Young N, and Coole L (2017). Risk factors for pertussis in adults and teenagers in England. Epidemiol. Infect 145, 1025–1036. 10.1017/S0950268816002983. [PubMed: 28065204]

13. Scanlon KM, Snyder YG, Skerry C, and Carbonetti NH (2017). Fatal Pertussis in the Neonatal Mouse Model Is Associated with Pertussis Toxin-Mediated Pathology beyond the Airways. Infect. Immun 85, e00355–17. 10.1128/IAI.00355-17. [PubMed: 28784932]

14. Scanlon KM, Chen L, and Carbonetti NH (2022). Pertussis Toxin Promotes Pulmonary Hypertension in an Infant Mouse Model of *Bordetella pertussis* Infection. J. Infect. Dis 225, 172–176. 10.1093/infdis/jiab325. [PubMed: 34145457]

15. Paddock CD, Sanden GN, Cherry JD, Gal AA, Langston C, Tatti KM, Wu KH, Goldsmith CS, Greer PW, Montague JL, et al. (2008). Pathology and pathogenesis of fatal *Bordetella pertussis* infection in infants. Clin. Infect. Dis 47, 328–338. 10.1086/589753. [PubMed: 18558873]

16. Bridel S, Bouchez V, Brancotte B, Hauck S, Armatys N, Landier A, Mühle E, Guillot S, Toubiana J, Maiden MCJ, et al. (2022). A comprehensive resource for *Bordetella* genomic epidemiology and biodiversity studies. Nat. Commun 13, 3807. 10.1038/s41467-022-31517-8. [PubMed: 35778384]

17. Linz B, Ivanov YV, Preston A, Brinkac L, Parkhill J, Kim M, Harris SR, Goodfield LL, Fry NK, Gorringe AR, et al. (2016). Acquisition and loss of virulence-associated factors during genome evolution and speciation in three clades of *Bordetella* species. BMC Genom. 17, 767. 10.1186/s12864-016-3112-5.

18. Kilgore PE, Salim AM, Zervos MJ, and Schmitt HJ (2016). Pertussis: Microbiology, Disease, Treatment, and Prevention. Clin. Microbiol. Rev 29, 449–486. 10.1128/CMR.00083-15. [PubMed: 27029594]

19. Weigand MR, Peng Y, Batra D, Burroughs M, Davis JK, Knipe K, Loparev VN, Johnson T, Juieng P, Rowe LA, et al. (2019). Conserved Patterns of Symmetric Inversion in the Genome Evolution of *Bordetella* Respiratory Pathogen. mSystems 4, e00702–19. 10.1128/mSystems.00702-19. [PubMed: 31744907]

20. MacArthur I, Belcher T, King JD, Ramasamy V, Alhammadi M, and Preston A (2019). The evolution of *Bordetella pertussis* has selected for mutations of acr that lead to sensitivity to hydrophobic molecules and fatty acids. Emerg. Microbes Infect 8, 603–612. 10.1080/22221751.2019.1601502. [PubMed: 30966996]

21. Taylor-Mulneix DL, Hamidou Soumana I, Linz B, and Harvill ET (2017). Evolution of Bordetellae from Environmental Microbes to Human Respiratory Pathogens: Amoebae as a Missing Link. Front. Cell. Infect. Microbiol 7, 510. 10.3389/fcimb.2017.00510. [PubMed: 29322035]

22. Ma L, Linz B, Caulfield AD, Dewan KK, Rivera I, and Harvill ET (2022). Natural History and Ecology of Interactions Between *Bordetella* Species and Amoeba. Front. Cell. Infect. Microbiol 12, 798317. 10.3389/fcimb.2022.798317. [PubMed: 35223538]

23. Carbonetti NH (2007). Immunomodulation in the pathogenesis of *Bordetella pertussis* infection and disease. Curr. Opin. Pharmacol 7, 272–278. 10.1016/j.coph.2006.12.004. [PubMed: 17418639]

24. Gestal MC, Whitesides LT, and Harvill ET (2019). Integrated Signaling Pathways Mediate *Bordetella* Immunomodulation, Persistence, and Transmission. Trends Microbiol. 27, 118–130. 10.1016/j.tim.2018.09.010. [PubMed: 30661570]

25. Belcher T, Dubois V, Rivera-Millot A, Locht C, and Jacob-Dubuisson F (2021). Pathogenicity and virulence of *Bordetella pertussis* and its adaptation to its strictly human host. Virulence 12, 2608–2632. 10.1080/21505594.2021.1980987. [PubMed: 34590541]

26. Ahmad JN, and Sebo P (2020). Adenylate Cyclase Toxin Tinkering With Monocyte-Macrophage Differentiation. Front. Immunol 11, 2181. 10.3389/fimmu.2020.02181. [PubMed: 33013916]

27. Fedele G, Schiavoni I, Adkins I, Klimova N, and Sebo P (2017). Invasion of Dendritic Cells, Macrophages and Neutrophils by the *Bordetella* Adenylate Cyclase Toxin: A Subversive Move to Fool Host Immunity. Toxins 9, 293. 10.3390/toxins9100293. [PubMed: 28934122]

28. Gorgojo J, Scharrig E, Gómez RM, Harvill ET, and Rodríguez ME (2017). *Bordetella parapertussis* Circumvents Neutrophil Extracellular Bactericidal Mechanisms. PLoS One 12, e0169936. 10.1371/journal.pone.0169936. [PubMed: 28095485]

29. Kuwae A, Momose F, Nagamatsu K, Suyama Y, and Abe A (2016). BteA Secreted from the *Bordetella bronchiseptica* Type III Secetion System Induces Necrosis through an Actin Cytoskeleton Signaling Pathway and Inhibits Phagocytosis by Macrophages. PLoS One 11, e0148387. 10.1371/journal.pone.0148387. [PubMed: 26828590]
30. Bendor L, Weyrich LS, Linz B, Rolin OY, Taylor DL, Goodfield LL, Smallridge WE, Kennett MJ, and Harvill ET (2015). Type Six Secretion System of *Bordetella bronchiseptica* and Adaptive Immune Components Limit Intracellular Survival During Infection. PLoS One 10, e0140743. 10.1371/journal.pone.0140743. [PubMed: 26485303]
31. Soumana IH, Dewan KK, Linz B, Rivera I, Ma L, Howard LK, Caulfield AD, Sedney CJ, Blas-Machado U, Sebo P, and Harvill ET (2022). Modeling the catarrhal stage of *Bordetella pertussis* upper respiratory tract infections in mice. Dis. Model. Mech 15, dmm049266. 10.1242/dmm.049266. [PubMed: 35311902]
32. Casadevall A, and Pirofski LA (2018). What Is a Host? Attributes of Individual Susceptibility. Infect. Immun 86, e00636–17. 10.1128/IAI.00636-17. [PubMed: 29084893]
33. Casadevall A, and Pirofski LA (2003). The damage-response framework of microbial pathogenesis. Nat. Rev. Microbiol 1, 17–24. 10.1038/nrmicro732. [PubMed: 15040176]
34. Mills KHG, and Gerdts V (2014). Mouse and pig models for studies of natural and vaccine-induced immunity to *Bordetella pertussis*. J. Infect. Dis 209, S16–S19. 10.1093/infdis/jit488. [PubMed: 24626866]
35. Holban AM, Gregoire CM, and Gestal MC (2022). Conquering the host: *Bordetella* spp. and *Pseudomonas aeruginosa* molecular regulators in lung infection. Front. Microbiol 13, 983149. 10.3389/fmicb.2022.983149. [PubMed: 36225372]
36. Cotter PA, and Miller JF (1994). BvgAS-mediated signal transduction: analysis of phase-locked regulatory mutants of *Bordetella bronchiseptica* in a rabbit model. Infect. Immun 62, 3381–3390. [PubMed: 8039908]
37. Mattoo S, Yuk MH, Huang LL, and Miller JF (2004). Regulation of type III secretion in Bordetella. Mol. Microbiol 52, 1201–1214. 10.1111/j.1365-2958.2004.04053.x. [PubMed: 15130135]
38. Gestal MC, Howard LK, Dewan K, Johnson HM, Barbier M, Bryant C, Soumana IH, Rivera I, Linz B, Blas-Machado U, and Harvill ET (2019). Enhancement of immune response against *Bordetella* spp. by disrupting immunomodulation. Sci. Rep 9, 20261. 10.1038/s41598-019-56652-z. [PubMed: 31889098]
39. Gestal MC, Howard LK, Dewan KK, and Harvill ET (2022). Bbvac: A Live Vaccine Candidate That Provides Long-Lasting Anamnestic and Th17-Mediated Immunity against the Three Classical. mSphere 7, e0089221. 10.1128/msphere.00892-21. [PubMed: 35196124]
40. Gestal MC, Blas-Machado U, Johnson HM, Rubin LN, Dewan KK, Bryant C, Tiemeyer M, and Harvill ET (2020). Disrupting *Bordetella* Immunosuppression Reveals a Role for Eosinophils in Coordinating the Adaptive Immune Response in the Respiratory Tract. Microorganisms 8, 1808. 10.3390/microorganisms8111808. [PubMed: 33212993]
41. Ondari E, Calvino-Sanles E, First NJ, and Gestal MC (2021). Eosinophils and Bacteria, the Beginning of a Story. Int. J. Mol. Sci 22, 8004. 10.3390/ijms22158004. [PubMed: 34360770]
42. Jacobsen EA, Helmers RA, Lee JJ, and Lee NA (2012). The expanding role(s) of eosinophils in health and disease. Blood 120, 3882–3890. 10.1182/blood-2012-06-330845. [PubMed: 22936660]
43. Jackson DJ, Akuthota P, and Roufosse F (2022). Eosinophils and eosinophilic immune dysfunction in health and disease. Eur. Respir. Rev 31, 210150. 10.1183/16000617.0150-2021. [PubMed: 35082127]
44. Simon HU, Yousefi S, Germic N, Arnold IC, Haczku A, Karaulov AV, Simon D, and Rosenberg HF (2020). The Cellular Functions of Eosinophils: Collegium Internationale Allergologicum (CIA) Update 2020. Int. Arch. Allergy Immunol 181, 11–23. 10.1159/000504847. [PubMed: 31786573]
45. DeChatelet LR, Migler RA, Shirley PS, Muss HB, Szejda P, and Bass DA (1978). Comparison of intracellular bactericidal activities of human neutrophils and eosinophils. Blood 52, 609–617. [PubMed: 678676]

46. Arnold IC, Artola-Borán M, Tallón de Lara P, Kyburz A, Taube C, Ottemann K, van den Broek M, Yousefi S, Simon HU, and Müller A (2018). Eosinophils suppress Th1 responses and restrict bacterially induced gastrointestinal inflammation. J. Exp. Med 215, 2055–2072. 10.1084/jem.20172049. [PubMed: 29970473]
47. Bohrer AC, Castro E, Hu Z, Queiroz ATL, Tocheny CE, Assmann M, Sakai S, Nelson C, Baker PJ, Ma H, et al. (2021). Eosinophils are part of the granulocyte response in tuberculosis and promote host resistance in mice. J. Exp. Med 218, e20210469. 10.1084/jem.20210469. [PubMed: 34347010]
48. Prince L, Martín-Faivre L, Villeret B, Sanchez-Guzman D, Le Guen P, Sallenave JM, and Garcia-Verdugo I (2023). Eosinophils Recruited during Pulmonary Vaccination Regulate Mucosal Antibody Production. Am. J. Respir. Cell Mol. Biol 68, 186–200. 10.1165/rcmb.2022-0236OC. [PubMed: 36194580]
49. Rubin K, and Glazer S (2018). The pertussis hypothesis: *Bordetella pertussis* colonization in the etiology of asthma and diseases of allergic sensitization. Med. Hypotheses 120, 101–115. 10.1016/j.mehy.2018.08.006. [PubMed: 30220328]
50. Ennis DP, Cassidy JP, and Mahon BP (2005). Acellular pertussis vaccine protects against exacerbation of allergic asthma due to *Bordetella pertussis* in a murine model. Clin. Diagn. Lab. Immunol 12, 409–417. 10.1128/CDLI.12.3.409-417.2005. [PubMed: 15753254]
51. Belcher T, Ait-Yahia S, Solans L, Debrie AS, Cauchi S, Tsicopoulos A, and Locht C (2022). Live attenuated pertussis vaccine for prevention and treatment of allergic airway inflammation in mice. NPJ Vaccines 7, 66. 10.1038/s41541-022-00494-w. [PubMed: 35739108]
52. Yu C, Cantor AB, Yang H, Browne C, Wells RA, Fujiwara Y, and Orkin SH (2002). Targeted deletion of a high-affinity GATA-binding site in the GATA-1 promoter leads to selective loss of the eosinophil lineage in vivo. J. Exp. Med 195, 1387–1395. 10.1084/jem.20020656. [PubMed: 12045237]
53. Ochkur SI, Doyle AD, Jacobsen EA, LeSuer WE, Li W, Protheroe CA, Zellner KR, Colbert D, Shen HH, Irvin CG, et al. (2017). Frontline Science: Eosinophil-deficient MBP-1 and EPX double-knockout mice link pulmonary remodeling and airway dysfunction with type 2 inflammation. J. Leukoc. Biol 102, 589–599. 10.1189/jlb.3HI1116-488RR. [PubMed: 28515227]
54. McDevitt MA, Shivdasani RA, Fujiwara Y, Yang H, and Orkin SH (1997). A "knockdown" mutation created by cis-element gene targeting reveals the dependence of erythroid cell maturation on the level of transcription factor GATA-1. Proc. Natl. Acad. Sci. USA 94, 6781–6785. 10.1073/pnas.94.13.6781. [PubMed: 9192642]
55. Warfel JM, and Merkel TJ (2013). Bordetella pertussis infection induces a mucosal IL-17 response and long-lived Th17 and Th1 immune memory cells in nonhuman primates. Mucosal Immunol. 6, 787–796. 10.1038/mi.2012.117. [PubMed: 23187316]
56. Raeven RHM, Brummelman J, van der Maas L, Tilstra W, Pennings JLA, Han WGH, van Els CACM, van Riet E, Kersten GFA, and Metz B (2016). Immunological Signatures after *Bordetella pertussis* Infection Demonstrate Importance of Pulmonary Innate Immune Cells. PLoS One 11, e0164027. 10.1371/journal.pone.0164027. [PubMed: 27711188]
57. Raeven RHM, Brummelman J, Pennings JLA, Nijst OEM, Kuipers B, Blok LER, Helm K, van Riet E, Jiskoot W, van Els CACM, et al. (2014). Molecular signatures of the evolving immune response in mice following a *Bordetella pertussis* infection. PLoS One 9, e104548. 10.1371/journal.pone.0104548. [PubMed: 25137043]
58. da Silva Antunes R, Babor M, Carpenter C, Khalil N, Cortese M, Mentzer AJ, Seumois G, Petro CD, Purcell LA, Vijayanand P, et al. (2018). Th1/Th17 polarization persists following whole-cell pertussis vaccination despite repeated acellular boosters. J. Clin. Invest 128, 3853–3865. 10.1172/JCI121309. [PubMed: 29920186]
59. Burdin N, Handy LK, and Plotkin SA (2017). What Is Wrong with Pertussis Vaccine Immunity? The Problem of Waning Effectiveness of Pertussis Vaccines. Cold Spring Harb. Perspect. Biol 9, a029454. 10.1101/cshperspect.a029454. [PubMed: 28289064]
60. Rangel-Moreno J, Moyron-Quiroz JE, Hartson L, Kusser K, and Randall TD (2007). Pulmonary expression of CXC chemokine ligand 13, CC chemokine ligand 19, and CC chemokine ligand 21 is essential for local immunity to influenza. Proc. Natl. Acad. Sci. USA 104, 10577–10582. 10.1073/pnas.0700591104. [PubMed: 17563386]

61. Chiavolini D, Rangel-Moreno J, Berg G, Christian K, Oliveira-Nascimento L, Weir S, Alroy J, Randall TD, and Wetzler LM (2010). Bronchus-associated lymphoid tissue (BALT) and survival in a vaccine mouse model of tularemia. PLoS One 5, e11156. 10.1371/journal.pone.0011156. [PubMed: 20585390]
62. Teillaud JL, Regard L, Martin C, Sibéril S, and Burgel PR (2018). Exploring the Role of Tertiary Lymphoid Structures Using a Mouse Model of Bacteria-Infected Lungs. Methods Mol. Biol 1845, 223–239. 10.1007/978-1-4939-8709-2_13. [PubMed: 30141016]
63. Bery AI, Shepherd HM, Li W, Krupnick AS, Gelman AE, and Kreisel D (2022). Role of tertiary lymphoid organs in the regulation of immune responses in the periphery. Cell. Mol. Life Sci 79, 359. 10.1007/s00018-022-04388-x. [PubMed: 35689679]
64. Wasbotten RK, Dahler AA, Mackel JJ, Morffy Smith C, and Rosen DA (2022). Murine Respiratory Tract Infection with Classical *Klebsiella pneumoniae* Induces Bronchus-Associated Lymphoid Tissue. Infect. Immun 90, e0059621. 10.1128/iai.00596-21. [PubMed: 35311545]
65. Silva-Sanchez A, and Randall TD (2020). Role of iBALT in Respiratory Immunity. Curr. Top. Microbiol. Immunol 426, 21–43. 10.1007/82_2019_191. [PubMed: 31974759]
66. Rangel-Moreno J, Hartson L, Navarro C, Gaxiola M, Selman M, and Randall TD (2006). Inducible bronchus-associated lymphoid tissue (iBALT) in patients with pulmonary complications of rheumatoid arthritis. J. Clin. Invest 116, 3183–3194. 10.1172/JCI28756. [PubMed: 17143328]
67. Ohtani O, and Ohtani Y (2008). Organization and developmental aspects of lymphatic vessels. Arch. Histol. Cytol 71, 1–22. 10.1679/aohc.71.1. [PubMed: 18622090]
68. Kawamata N, Xu B, Nishijima H, Aoyama K, Kusumoto M, Takeuchi T, Tei C, Michie SA, and Matsuyama T (2009). Expression of endothelia and lymphocyte adhesion molecules in bronchus-associated lymphoid tissue (BALT) in adult human lung. Respir. Res 10, 97. 10.1186/1465-9921-10-97. [PubMed: 19845971]
69. Hwang JY, Randall TD, and Silva-Sanchez A (2016). Inducible Bronchus-Associated Lymphoid Tissue: Taming Inflammation in the Lung. Front. Immunol 7, 258. 10.3389/fimmu.2016.00258. [PubMed: 27446088]
70. Kendall MM (2017). Extra! Extracellular Effector Delivery into Host Cells via the Type 3 Secretion System. mBio 8, e00594–17. 10.1128/mBio.00594-17. [PubMed: 28465427]
71. Yuk MH, Harvill ET, Cotter PA, and Miller JF (2000). Modulation of host immune responses, induction of apoptosis and inhibition of NF-kappaB activation by the Bordetella type III secretion system. Mol. Microbiol 35, 991–1004. [PubMed: 10712682]
72. Kamanova J (2020). Type III Secretion Injectosome and Effector Proteins. Front. Cell. Infect. Microbiol 10, 466. 10.3389/fcimb.2020.00466. [PubMed: 33014891]
73. Nicholson TL, Brockmeier SL, Loving CL, Register KB, Kehrli ME, and Shore SM (2014). The *Bordetella bronchiseptica* type III secretion system is required for persistence and disease severity but not transmission in swine. Infect. Immun 82, 1092–1103. 10.1128/IAI.01115-13. [PubMed: 24366249]
74. Mai E, Limkar AR, Percopo CM, and Rosenberg HF (2021). Generation of Mouse Eosinophils in Tissue Culture from Unselected Bone Marrow Progenitors. Methods Mol. Biol 2241, 37–47. 10.1007/978-1-0716-1095-4_4. [PubMed: 33486726]
75. Chu VT, Beller A, Rausch S, Strandmark J, Zänker M, Arbach O, Kruglov A, and Berek C (2014). Eosinophils promote generation and maintenance of immunoglobulin-A-expressing plasma cells and contribute to gut immune homeostasis. Immunity 40, 582–593. 10.1016/j.immuni.2014.02.014. [PubMed: 24745334]
76. Aazami H, Seif F, Ghalehbaghi B, Babaheidarian P, Mohebbi A, Ahmadi A, Khoshmirsafa M, Ghalehbaghi S, Behnam B, Entezami KZ, et al. (2020). Local eosinophils are associated with increased IgA subclass levels in the sinonasal mucosa of chronic rhinosinusitis with polyp patients. Allergy Asthma Clin. Immunol 16, 30. 10.1186/s13223-020-00428-y. [PubMed: 32351585]
77. Blosse A, Peru S, Levy M, Marteyn B, Floch P, Sifré E, Giese A, Prochazkova-Carlotti M, Azzi Martin L, Dubus P, et al. (2020). APRIL-producing eosinophils are involved in gastric MALT lymphomagenesis induced by *Helicobacter* sp infection. Sci. Rep 10, 14858. 10.1038/s41598-020-71792-3. [PubMed: 32908188]

78. Tian Y, Terkawi MA, Onodera T, Alhasan H, Matsumae G, Takahashi D, Hamasaki M, Ebata T, Aly MK, Kida H, et al. (2020). Blockade of XCL1/Lymphotactin Ameliorates Severity of Periprosthetic Osteolysis Triggered by Polyethylene-Particles. Front. Immunol 11, 1720. 10.3389/fimmu.2020.01720. [PubMed: 32849609]

79. Miller MA, Stabenow JM, Parvathareddy J, Wodowski AJ, Fabrizio TP, Bina XR, Zalduondo L, and Bina JE (2012). Visualization of murine intranasal dosing efficiency using luminescent *Francisella tularensis:* effect of instillation volume and form of anesthesia. PLoS One 7, e31359. 10.1371/journal.pone.0031359. [PubMed: 22384012]

80. Dewan KK, Linz B, DeRocco SE, and Harvill ET (2020). Acellular Pertussis Vaccine Components: Today and Tomorrow. Vaccines 8. 10.3390/vaccines8020217.

81. Belchior E, Guillot S, Poujol I, Thabuis A, Chouin L, Martel M, Delisle E, Six C, Guiso N, and Lévy-Bruhl D (2020). Comparison of whole-cell versus acellular pertussis vaccine effectiveness in school clusters of pertussis, France, 2013. Med. Mal. Infect 50, 617–619. 10.1016/j.medmal.2020.07.004. [PubMed: 32659333]

82. Borkner L, Curham LM, Wilk MM, Moran B, and Mills KHG (2021). Correction: IL-17 mediates protective immunity against nasal infection with *Bordetella pertussis* by mobilizing neutrophils, especially Siglec-F. Mucosal Immunol. 14, 1218–1219. 10.1038/s41385-021-00417-3. [PubMed: 34079070]

83. Borkner L, Curham LM, Wilk MM, Moran B, and Mills KHG (2021). IL-17 mediates protective immunity against nasal infection with *Bordetella pertussis* by mobilizing neutrophils, especially Siglec-F. Mucosal Immunol. 14, 1183–1202. 10.1038/s41385-021-00407-5. [PubMed: 33976385]

84. Grisaru-Tal S, Rothenberg ME, and Munitz A (2022). Eosinophil-lymphocyte interactions in the tumor microenvironment and cancer immunotherapy. Nat. Immunol 23, 1309–1316. 10.1038/s41590-022-01291-2. [PubMed: 36002647]

85. Williams TL, Rada B, Tandon E, and Gestal MC (2020). "NETs and EETs, a Whole Web of Mess". Microorganisms 8. 10.3390/microorganisms8121925.

86. Yousefi S, Simon D, Stojkov D, Karsonova A, Karaulov A, and Simon HU (2020). In vivo evidence for extracellular DNA trap formation. Cell Death Dis. 11, 300. 10.1038/s41419-020-2497-x. [PubMed: 32355207]

87. Krishack PA, Louviere TJ, Decker TS, Kuzel TG, Greenberg JA, Camacho DF, Hrusch CL, Sperling AI, and Verhoef PA (2019). Protection against *Staphylococcus aureus* bacteremia-induced mortality depends on ILC2s and eosinophils. JCI Insight 4, e124168. 10.1172/jci.insight.124168. [PubMed: 30721149]

88. Gurtner A, Gonzalez-Perez I, and Arnold IC (2021). Intestinal eosinophils, homeostasis and response to bacterial intrusion. Semin. Immunopathol 43, 295–306. 10.1007/s00281-021-00856-x. [PubMed: 33929602]

89. Linch SN, Kelly AM, Danielson ET, Pero R, Lee JJ, and Gold JA (2009). Mouse eosinophils possess potent antibacterial properties in vivo. Infect. Immun 77, 4976–4982. 10.1128/IAI.00306-09. [PubMed: 19703974]

90. Davido B, Makhloufi S, Matt M, Calin R, Senard O, Perronne C, Dinh A, and Salomon J (2017). Changes in eosinophil count during bacterial infection: revisiting an old marker to assess the efficacy of anti-microbial therapy. Int. J. Infect. Dis 61, 62–66. 10.1016/j.ijid.2017.06.005. [PubMed: 28627430]

91. Persson T, Andersson P, Bodelsson M, Laurell M, Malm J, and Egesten A (2001). Bactericidal activity of human eosinophilic granulocytes against *Escherichia coli*. Infect. Immun 69, 3591–3596. 10.1128/IAI.69.6.3591-3596.2001. [PubMed: 11349018]

92. Yazdanbakhsh M, Eckmann CM, Bot AA, and Roos D (1986). Bactericidal action of eosinophils from normal human blood. Infect. Immun 53, 192–198. 10.1128/IAI.53.1.192-198.1986. [PubMed: 3522428]

93. Bayram J, Malcova I, Sinkovec L, Holubova J, Streparola G, Jurnecka D, Kucera J, Sedlacek R, Sebo P, and Kamanova J (2020). Cytotoxicity of the effector protein BteA was attenuated in *Bordetella pertussis* by insertion of an alanine residue. PLoS Pathog. 16, e1008512. 10.1371/journal.ppat.1008512. [PubMed: 32776984]

94. August A, and Marichal T (2023). Eosinophils and Lung Mucosal Antibody Production: Is Location the Key? Am. J. Respir. Cell Mol. Biol 68, 124–126. 10.1165/rcmb.2022-0410ED. [PubMed: 36306503]

95. Travers J, and Rothenberg ME (2015). Eosinophils in mucosal immune responses. Mucosal Immunol 8, 464–475. 10.1038/mi.2015.2. [PubMed: 25807184]

96. Berek C. (2016). Eosinophils: important players in humoral immunity. Clin. Exp. Immunol 183, 57–64. 10.1111/cei.12695. [PubMed: 26291602]

97. Liu Y, Tangsun Y, Xiao Y, Zhang D, and Cao M (2016). Pulmonary infiltration with eosinophilia complicated with mucosa-associated lymphoid tissue lymphoma: A case report. Oncol. Lett 12, 1818–1820. 10.3892/ol.2016.4841. [PubMed: 27588128]

98. Yoshimura K, Ohge H, Uegami S, Watadani Y, Hirano T, and Takahashi S (2021). Small intestinal mucosa-associated lymphoid tissue lymphoma with deep ulcer and severe stenosis: A case report. Int. J. Surg. Case Rep 88, 106539. 10.1016/j.ijscr.2021.106539. [PubMed: 34741855]

99. Navarrete KM, Bumba L, Prudnikova T, Malcova I, Allsop TR, Sebo P, and Kamanova J (2023). BopN is a Gatekeeper of the *Bordetella* Type III Secretion System. Microbiol. Spectr 11, e0411222. 10.1128/spectrum.04112-22. [PubMed: 37036369]

100. Medici NP, and Bliska JB (2019). Methods for Detection of Pyrin Inflammasome Assembly in Macrophages Infected with *Yersinia* spp. Methods Mol. Biol 2010, 241–255. 10.1007/978-1-4939-9541-7_17. [PubMed: 31177443]

101. Chung LK, Park YH, Zheng Y, Brodsky IE, Hearing P, Kastner DL, Chae JJ, and Bliska JB (2016). The *Yersinia* Virulence Factor YopM Hijacks Host Kinases to Inhibit Type III Effector-Triggered Activation of the Pyrin Inflammasome. Cell Host Microbe 20, 296–306. 10.1016/j.chom.2016.07.018. [PubMed: 27569559]

102. Seder RA, Darrah PA, and Roederer M (2008). T-cell quality in memory and protection: implications for vaccine design. Nat. Rev. Immunol 8, 247–258. 10.1038/nri2274. [PubMed: 18323851]

103. Darrah PA, Patel DT, De Luca PM, Lindsay RWB, Davey DF, Flynn BJ, Hoff ST, Andersen P, Reed SG, Morris SL, et al. (2007). Multifunctional TH1 cells define a correlate of vaccine-mediated protection against *Leishmania* major. Nat. Med 13, 843–850. 10.1038/nm1592. [PubMed: 17558415]

104. da Silva Antunes R, Garrigan E, Quiambao LG, Dhanda SK, Marrama D, Westernberg L, Wang E, Abawi A, Sutherland A, Armstrong SK, et al. (2023). T cell reactivity to *Bordetella pertussis* is highly diverse regardless of childhood vaccination. Cell Host Microbe 31, 1404–1416.e4. 10.1016/j.chom.2023.06.015. [PubMed: 37490913]

105. Dirix V, Verscheure V, Vermeulen F, De Schutter I, Goetghebuer T, Locht C, and Mascart F (2012). Both $CD4^+$ and $CD8^+$ lymphocytes participate in the IFN-γ response to filamentous hemagglutinin from *Bordetella pertussis* in infants, children, and adults. Clin. Dev. Immunol 2012, 795958. 10.1155/2012/795958. [PubMed: 22550536]

106. Wong TW, Doyle AD, Lee JJ, and Jelinek DF (2014). Eosinophils regulate peripheral B cell numbers in both mice and humans. J. Immunol 192, 3548–3558. 10.4049/jimmunol.1302241. [PubMed: 24616476]

107. Akuthota P, Wang HB, Spencer LA, and Weller PF (2008). Immunoregulatory roles of eosinophils: a new look at a familiar cell. Clin. Exp. Allergy 38, 1254–1263. 10.1111/j.1365-2222.2008.03037.x. [PubMed: 18727793]

108. Wen T, and Rothenberg ME (2016). The Regulatory Function of Eosinophils. Microbiol. Spectr 4. 10.1128/microbiolspec.MCHD-0020-2015.

109. Amin K, Issa SM, Ali KM, Aziz MI, Hama Amieen HM, Bystrom J, and Janson C (2020). Evidence for eosinophil and IL-17 mediated inflammation in allergic rhinitis. Clin. Mol. Allergy 18, 6. 10.1186/s12948-020-00117-6. [PubMed: 32280308]

110. Dias PM, and Banerjee G (2013). The role of Th17/IL-17 on eosinophilic inflammation. J. Autoimmun 40, 9–20. 10.1016/j.jaut.2012.07.004. [PubMed: 22906357]

111. Malacco N.L.S.d.O., Rachid MA, Gurgel ILDS, Moura TR, Sucupira PHF, de Sousa LP, de Souza DDG, Russo R.d.C., Teixeira MM, and Soriani FM (2018). Eosinophil-Associated Innate IL-17

Response Promotes *Aspergillus fumigatus* Lung Pathology. Front. Cell. Infect. Microbiol 8, 453. 10.3389/fcimb.2018.00453. [PubMed: 30687649]

112. Hosoki K, Nakamura A, Nagao M, Hiraguchi Y, Tanida H, Tokuda R, Wada H, Nobori T, Suga S, and Fujisawa T (2012). *Staphylococcus aureus* directly activates eosinophils via platelet-activating factor receptor. J. Leukoc. Biol 92, 333–341. 10.1189/jlb.0112009. [PubMed: 22595142]
113. Tesfaye DY, Bobic S, Lysén A, Huszthy PC, Gudjonsson A, Braathen R, Bogen B, and Fossum E (2022). Targeting Xcr1 on Dendritic Cells Rapidly Induce Th1-Associated Immune Responses That Contribute to Protection Against Influenza Infection. Front. Immunol 13, 752714. 10.3389/fimmu.2022.752714. [PubMed: 35296089]
114. Yuk MH, Harvill ET, and Miller JF (1998). The BvgAS virulence control system regulates type III secretion in Bordetella bronchiseptica. Mol. Microbiol 28, 945–959. [PubMed: 9663681]
115. Jackson SJ, Andrews N, Ball D, Bellantuono I, Gray J, Hachoumi L, Holmes A, Latcham J, Petrie A, Potter P, et al. (2017). Does age matter? The impact of rodent age on study outcomes. Lab. Anim 51, 160–169. 10.1177/0023677216653984. [PubMed: 27307423]
116. Ardanuy J, Scanlon K, Skerry C, Fuchs SY, and Carbonetti NH (2020). Age-Dependent Effects of Type I and Type III IFNs in the Pathogenesis of. J. Immunol 204, 2192–2202. 10.4049/jimmunol.1900912. [PubMed: 32152071]
117. Stainer DW, and Scholte MJ (1970). A simple chemically defined medium for the production of phase I *Bordetella pertussis*. J. Gen. Microbiol 63, 211–220. 10.1099/00221287-63-2-211. [PubMed: 4324651]
118. Gestal MC, Rivera I, Howard LK, Dewan KK, Soumana IH, Dedloff M, Nicholson TL, Linz B, and Harvill ET (2018). Blood or Serum Exposure Induce Global Transcriptional Changes, Altered Antigenic Profile, and Increased Cytotoxicity by Classical Bordetellae. Front. Microbiol 9, 1969. 10.3389/fmicb.2018.01969. [PubMed: 30245672]
119. Davenport ML, Sherrill TP, Blackwell TS, and Edmonds MD (2020). Perfusion and Inflation of the Mouse Lung for Tumor Histology. J. Vis. Exp 10.3791/60605.
120. Amirouche A, Ait-Ali D, Nouri H, Boudrahme-Hannou L, Tliba S, Ghidouche A, and Bitam I (2021). TRIzol-based RNA extraction for detection protocol for SARS-CoV-2 of coronavirus disease 2019. New Microbes New Infect. 41, 100874. 10.1016/j.nmni.2021.100874. [PubMed: 33815807]
121. Cossarizza A, Chang HD, Radbruch A, Acs A, Adam D, Adam-Klages S, Agace WW, Aghaeepour N, Akdis M, Allez M, et al. (2019). Guidelines for the use of flow cytometry and cell sorting in immunological studies (second edition). Eur. J. Immunol 49, 1457–1973. 10.1002/eji.201970107. [PubMed: 31633216]
122. Zwolinska K, Bienkowska-Haba M, Scott RS, Keiffer T, and Sapp M (2023). Experimental Support for Human Papillomavirus Genome Amplification Early after Infectious Delivery. J. Virol 97, e0021423. 10.1128/jvi.00214-23. [PubMed: 37223953]
123. Mishra P, Pandey CM, Singh U, Keshri A, and Sabaretnam M (2019). Selection of appropriate statistical methods for data analysis. Ann. Card Anaesth 22, 297–301. 10.4103/aca.ACA_248_18. [PubMed: 31274493]
124. Festing MFW, and Altman DG (2002). Guidelines for the design and statistical analysis of experiments using laboratory animals. ILAR J. 43, 244–258. 10.1093/ilar.43.4.244. [PubMed: 12391400]
125. Charan J, and Kantharia ND (2013). How to calculate sample size in animal studies? J. Pharmacol. Pharmacother 4, 303–306. 10.4103/0976-500X.119726. [PubMed: 24250214]
126. Lenth RV (2007). Statistical power calculations. J. Anim. Sci 85, E24–E29. 10.2527/jas.2006-449. [PubMed: 17060421]
127. Abu Bakar ZH, Bellier JP, Wan Ngah WZ, Yanagisawa D, Mukaisho KI, and Tooyama I (2023). Optimization of 3D Immunofluorescence Analysis and Visualization Using IMARIS and MeshLab. Cells 12. 10.3390/cells12020218.
128. Taylor SC, Nadeau K, Abbasi M, Lachance C, Nguyen M, and Fenrich J (2019). The Ultimate qPCR Experiment: Producing Publication Quality, Reproducible Data the First Time. Trends Biotechnol. 37, 761–774. 10.1016/j.tibtech.2018.12.002. [PubMed: 30654913]

Highlights

- Eosinophils are required for clearance of *B. bronchiseptica* Δ*btrS* but not wild type
- *B. bronchiseptica* suppresses eosinophil functions via *btrS* to promote persistence
- Eosinophils facilitate the induction of iBALT, IL-17, and IgA
- Eosinophils mediate iBALT formation via XCL1 secretion

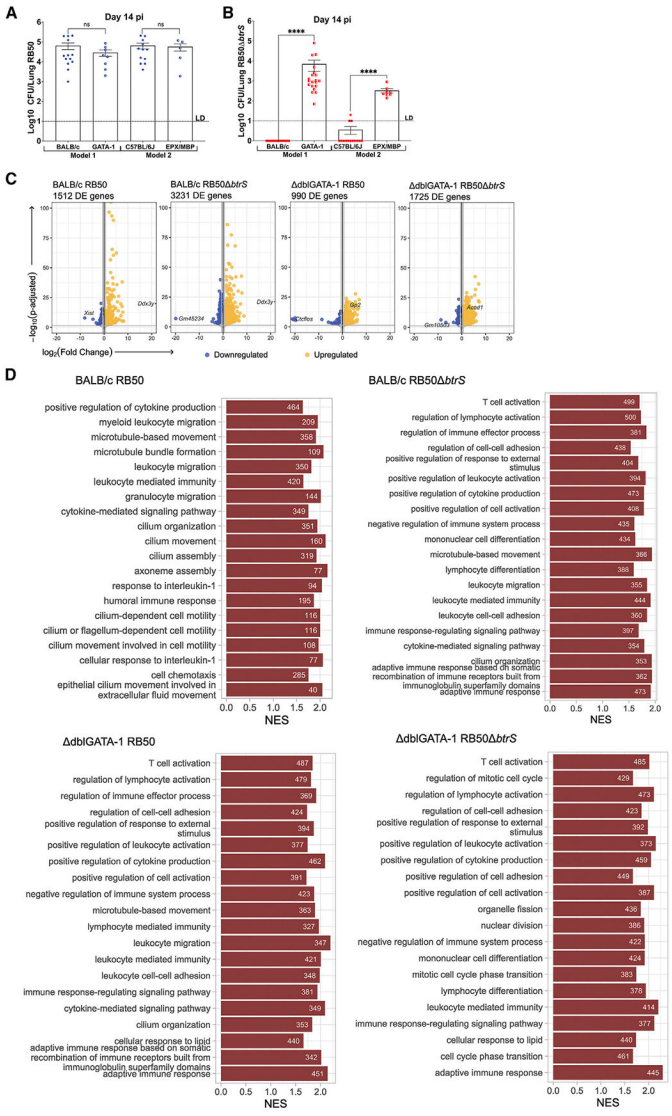

Figure 1. Eosinophils drive clearance of RB50Δ*btrS* but not wild-type *B. bronchiseptica* RB50

(A and B) BALB/c, ΔdblGATA-1, C57BL/6J, and *EPX/MBP*$^{-/-}$ mice were intranasally inoculated with PBS or PBS containing 5×10^5 RB50 (blue) (A) or RB50Δ*btrS* (red) (B). On day 14 post infection, lungs were harvested, and colony-forming units (CFU) were enumerated. Each dot represents an individual mouse (n = 5–20), and the columns represent the mean ± SEM. One-way ANOVA with Tukey's multiple-comparisons test was conducted. ****p < 0.0001; ns, non-significant.

(C and D) BALB/c and ΔdblGATA-1 mice were intranasally inoculated with PBS or PBS containing 5×10^5 RB50 or RB50Δ*btrS*. On day 7 post infection, lungs were collected for bulk RNA sequencing. Shown is representation of each group versus their respective uninfected controls. Colored dots represent DEGs (p adjusted < 0.05, absolute $\log_2$ fold change R 1.5; blue, downregulated; yellow, upregulated). Names of top upregulated and downregulated genes (fold change levels) are plotted for each comparison. The total number of DEGs is written on top of the graphic for each comparison (C). Shown is representation

of gene set enrichment analysis (GSEA) top 20 p-adjusted pathways of the biological process Gene Ontology (GO) category for each group, ordered by significance. The y axes represent normalized enrichment score (NES). Numbers inside bars indicate genes participating in core enrichment (D).

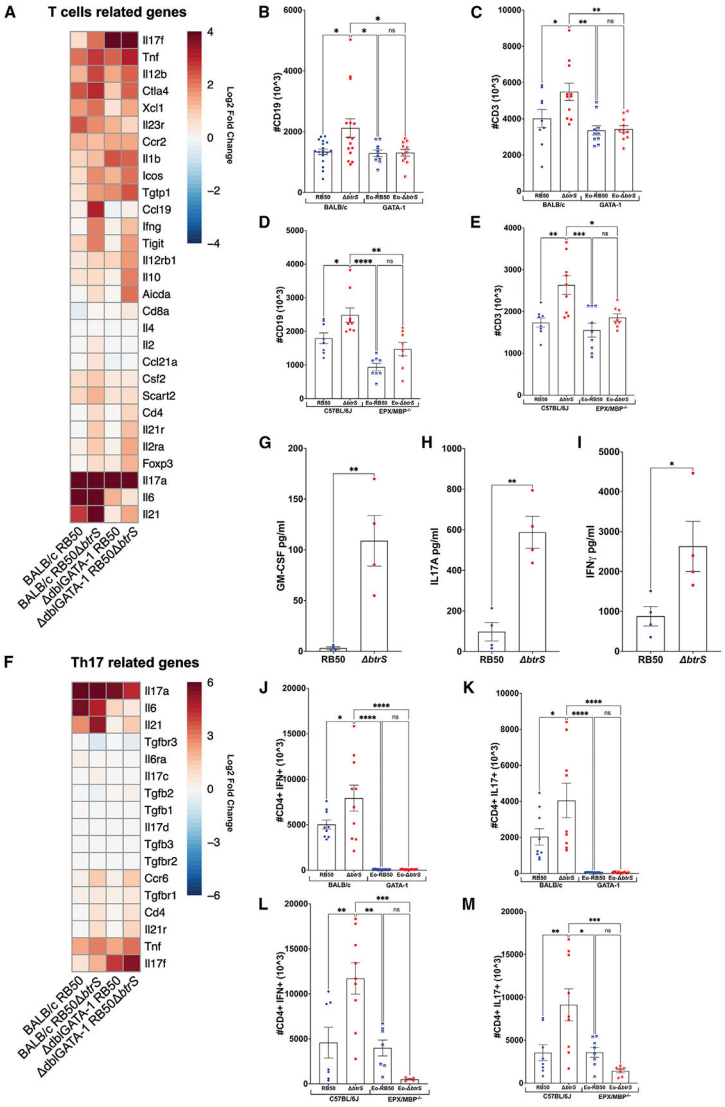

Figure 2. *btrS* suppresses an eosinophil-mediated adaptive immune response in the lungs

(A) BALB/c and ΔdblGATA-1 mice were intranasally challenged with PBS or PBS containing 5×10^5 RB50 or RB50Δ*btrS*. On day 7 post infection, lungs were collected to perform RNA sequencing. Shown is $\log_2$ fold change expression of genes correlated with T cell-related genes and specific CD4 and CD8 T cell markers (n = 3–5 mice per group).

(B–E) BALB/c - ΔdblGATA-1 (B and C) and C57BL/6J - *EPX/MBP*$^{-/-}$ (D and E) mice were intranasally challenged with PBS or 5×10^5 RB50 or RB50Δ*btrS*. On day 7 post infection, lungs were collected to perform flow cytometry staining using the surface marker CD19 for B cells (B and D) and CD3 for T cells (C and E). Each individual point represents one single animal (n = 9–18), and the columns represent the mean ± SEM. After running an outlier test, one-Way ANOVA with Tukey's multiple-comparisons test was performed. *p < 0.01, **p < 0.005, ***p < 0.001, and ****p < 0.0001.

(F) BALB/c and ΔdblGATA-1 mice were intranasally challenged with PBS or PBS containing 5×10^5 RB50 or RB50Δ*btrS*. Lungs were collected on day 7 post infection to extract RNA and perform bulk sequencing. Genes correlated with Th17 mucosal responses

were plotted on a heatmap, where darker red represents more expression, and darker blue represents less expression (n = 3–5 mice per group).

(G–I) BALB/c mice were intranasally challenged with PBS containing 5×10^5 RB50 or RB50Δ*btrS*. On day 7 post infection, lungs were collected to isolate single T cells. After 48-h stimulation with $CD3^+/CD28^+$ beads, secretome analysis was performed using the Isoplexis T cell CodePlex analysis, which included GM-SCF (G), IL-17A (H), and IFN-γ (I). The whole analysis is shown in Figure S3. Each individual point represents one individual animal (n = 4), and the columns represent the mean ± SEM. One-way ANOVA with Tukey's multiple-comparisons test was performed. *p < 0.01 and **p < 0.005.

(J–M) BALB/c - ΔdblGATA-1 (J and K) and C57BL/6J - *EPX/MBP*$^{-/-}$ (L and M) mice were intranasally challenged with PBS or PBS containing 5×10^5 RB50 or RB50Δ*btrS*. On day 7 post infection, lungs were collected to perform flow cytometry staining to enumerate $CD4^+IFN\gamma^+$ cells (J and L) and $CD4^+$ $IL\text{-}17^+$ cells (K and M). Each individual point represents one individual animal (n = 9–18), and the columns represent the mean ± SEM. One-way ANOVA with Tukey's multiple-comparisons test was performed. *p < 0.01, **p < 0.005, ***p < 0.001, and ****p < 0.0001.

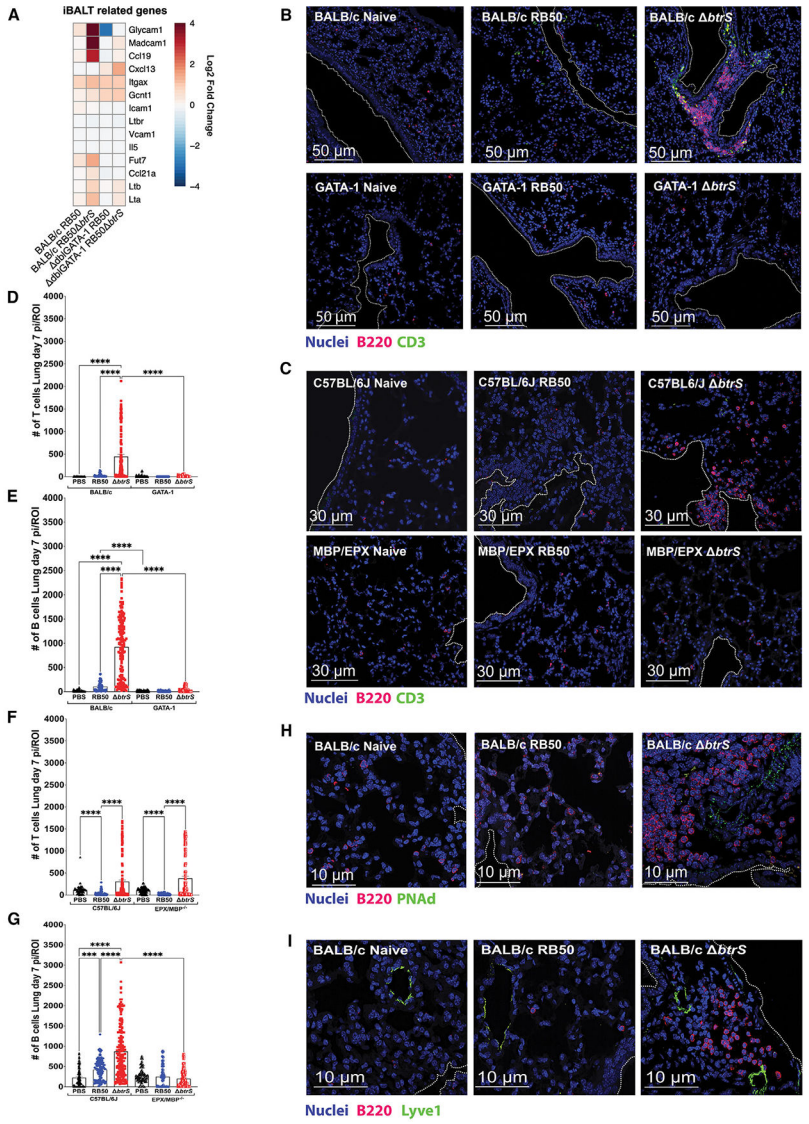

Figure 3. Eosinophils are required for iBALT formation during infection with the *btrS*-null *B. bronchiseptica* strain

(A) RNA sequencing was performed on the lungs of BALB/c and ΔdblGATA-1 mice left uninfected or infected with RB50 or RB50Δ*btrS* on day 7 post infection. The heatmap shows the expression levels of genes related to iBALT formation. The color scale represents log2 fold change values (n = 3–5 mice per group).

(B–G) BALB/c and ΔdblGATA-1 (B) and C57BL/6J and *EPX/MBP*$^{-/-}$ mice (C) were intranasally challenged with PBS or PBS containing 5 × 10^5 RB50 or RB50Δ*btrS*. On day 7 post infection, lungs were perfused and embedded in paraffin, and sections were stained with Hoechst (nucleus, blue), CD3 (T cells, green), and B220 (B cells, red). Images were obtained using an Olympus CSU W1 spinning disk microscope. Representative images for BALB/c and ΔdblGATA-1 mice (B) as well as for C57BL/6J and *EPX/MBP*$^{-/-}$ mice (C) are shown. T cells (D and F) and B cells (E and G) per region of interest are shown. Each individual point represents the number of positive cells per region of interest in each photo.

The columns represent the mean ± SEM. After running an outlier tests, two-way ANOVA with Tukey's multiple-comparisons test was performed. ****$p < 0.0001$.
(H) BALB/c mice were intranasally challenged with PBS or PBS containing 5×10^5 RB50 or RB50Δ*btrS*. On day 7 post infection, lungs were perfused and embedded in paraffin. Sections were stained with Hoechst (nucleus, blue), B220 (B cells, red), and pNAD high endothelial venules (green) and imaged using an Olympus spinning disk microscope.
(I) BALB/c mice were intranasally challenged with PBS or 5×10^5 RB50 or RB50Δ*btrS*. On day 7 post infection, lungs were perfused and paraffin embedded. Sections were stained with Hoechst (nucleus, blue), B220 (B cells, red), and Lyve-1 for lymphatic vessels (green) and imaged using an Olympus spinning disk microscope.

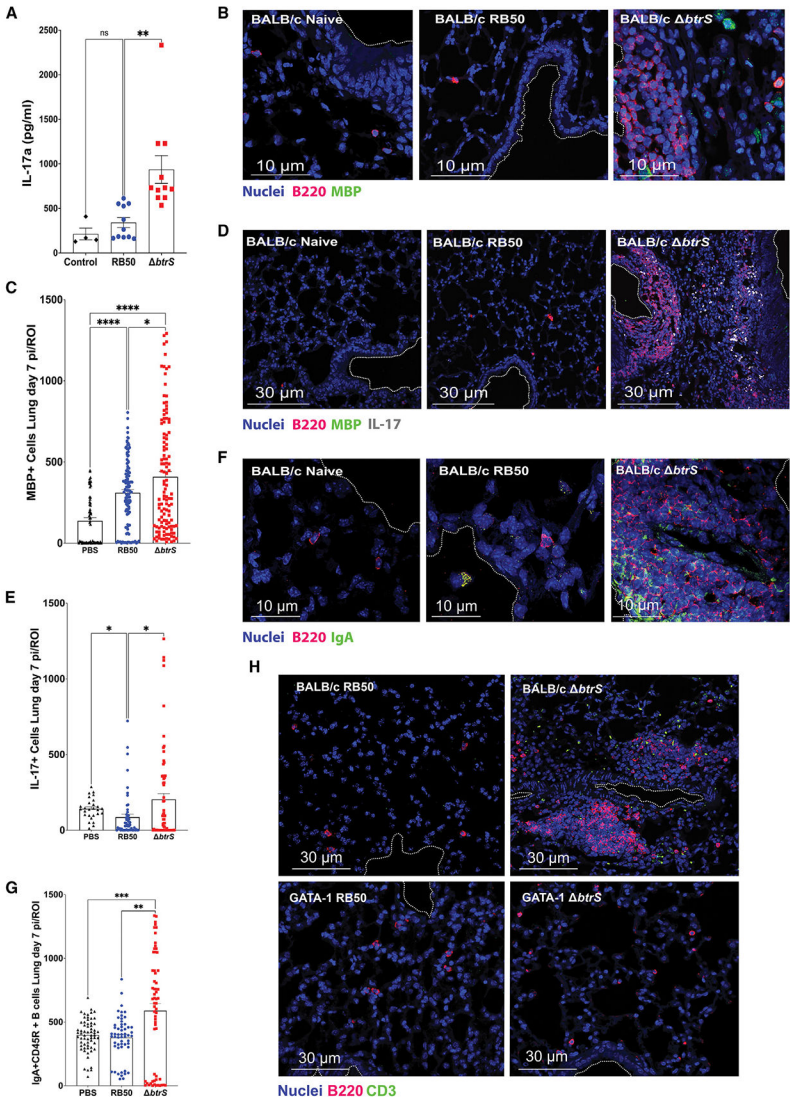

Figure 4. Eosinophils promote mucosal responses within the iBALT and the surrounding areas

(A) Bone marrow-derived eosinophils were mock challenged or co-cultured at an MOI of 10 with RB50 (blue) or RB50Δ*btrS* (red). At 4 h post infection, the supernatant was collected to determine the levels of IL-17a secreted to the medium. Each dot represents the mean of the 3–4 technical replicates, and the columns represent the mean ± SEM among the biological replicates. One-way ANOVA with Dunnett's test was performed using multiple comparisons. ****$p < 0.0001$.

(B and C) BALB/c mice were intranasally challenged with PBS or PBS containing 5×10^5 RB50 or RB50Δ*btrS*. On day 7 post infection, lungs were perfused and embedded in paraffin. Following sectioning, sections were stained with Hoechst (nucleus blue), B220 (B cells, red), and eosinophil major basic protein (MBP; green) and imaged using an Olympus CSU W1 spinning disk microscope. Representative images for BALB/c mice are shown (B). For the quantification, we imaged lungs from 6 mice per group, 3 sections per mouse, and 10 regions of interest (ROIs) in the Keyence microscope and used its own software for the quantification. Numbers of MBP cells per ROI are shown (C). Each individual

point represents the number of positive cells per ROI in each photo, and the columns represent the mean ± SEM. After running an outlier test, a two-way ANOVA with Tukey's multiple-comparisons test was performed. *$p < 0.01$ and ****$p < 0.0001$.

(D and E) BALB/c mice were intranasally challenged with PBS or 5×10^5 RB50 or RB50Δ*btrS*. On day 7 post infection, lungs were perfused and embedded in paraffin. Following sectioning, sections were stained with Hoechst (nucleus, blue), B220 (B cells, red), and IL-17 (white) and imaged using an Olympus CSU W1 spinning disk confocal system. Representative images for BALB/c mice are shown (D). For the quantification, we imaged lungs from 6 mice per group, 3 sections per mouse, and 10 ROIs in the Keyence microscope and used its own software for the quantification. Numbers of IL-17^+ cells per ROI were analyzed (E). Each individual point represents the number of positive cells per ROI in each photo, and the columns represent the mean ± SEM. After running an outlier test, a two-way ANOVA with Tukey's multiple-comparisons test was performed. *$p < 0.01$.

(F and G) BALB/c mice were intranasally challenged with PBS or PBS containing 5×10^5 RB50 or RB50Δ*btrS*. On day 7 post infection, lungs were perfused and embedded in paraffin. Following sectioning, sections were stained with Hoechst (nucleus, blue), B220 (B cells, red), and IgA (green) and imaged using an Olympus CSU W1 spinning disk confocal system. Representative images for BALB/c mice are shown (F). For the quantification, we imaged lungs from 6 mice per group, 3 sections per mouse, and 10 ROIs in the Keyence microscope and used its own software for the quantification. Shown are numbers of $CD45^+IgA^+$ cells per ROI (G). Each individual point represents the number of positive cells per ROI in each photo, and the columns represent the mean ± SEM. After running an outlier test, a two-way ANOVA with Tukey's multiple-comparisons test was performed. **$p < 0.005$ and ****$p < 0.0001$.

(H) BALB/c and ΔdblGATA-1 mice were intranasally challenged with PBS or 5×10^5 RB50 or RB50Δ*btrS*. On day 28 post infection, lungs were perfused and paraffin-embedded. Following sectioning, sections were stained with Hoechst (nucleus, blue), CD3 (T cells, green), and B220 (B cells, red) and imaged using an Olympus CSU W1 spinning disk confocal system.

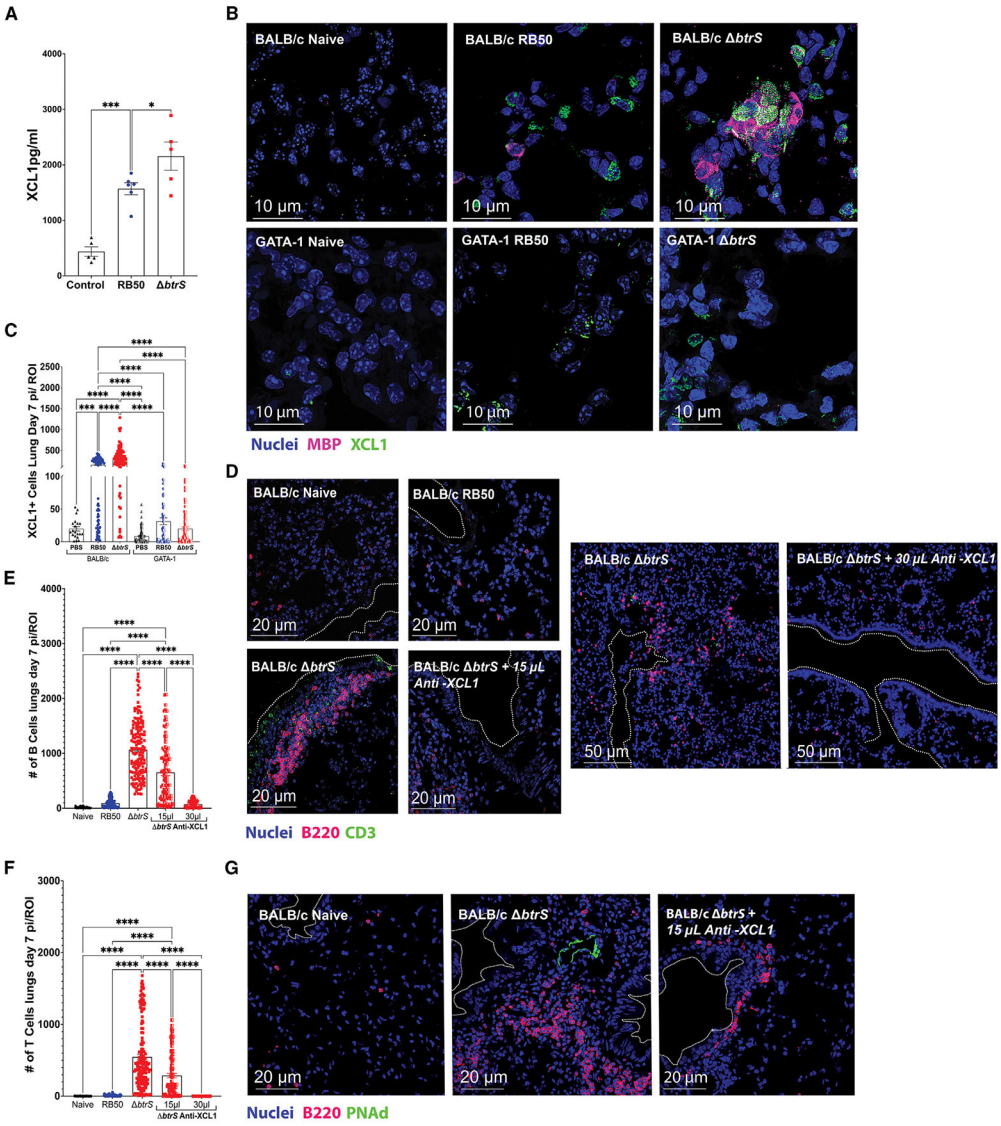

Figure 5. Eosinophil-derived XCL1 is required for iBALT formation

(A) Bone marrow-derived eosinophils were left unchallenged or inoculated at an MOI of 10 with RB50 (blue) or RB50Δ*btrS* (red). At 4 h post infection, the supernatant was collected to evaluate levels of XCL1. Each dot corresponds with the mean of the three technical replicates of one biological replicate, and the columns represent the mean ± SEM. One-way ANOVA with Dunnett's multiple-comparisons test was performed. **$p < 0.005$ and ***$p < 0.001$.

(B and C) BALB/c and ΔdblGATA-1 mice were intranasally challenged with PBS or PBS containing 5×10^5 RB50 or RB50Δ*btrS*. On day 7 post infection, lungs were perfused and embedded in paraffin. Following sectioning, samples were stained with Hoechst (nucleus, blue), eosinophil MBP (red), and XCL1 (green) and imaged using an Olympus CSU W1 spinning disk confocal system. Representative images for BALB/c mice (B) are shown. The graph shows the percentage of XCL1 in 3–4 mice with 2–5 images quantified per mouse (C). Each individual point represents the number of positive cells per ROI in each photo, and

the columns represent the mean ± SEM. An outlier test was followed by a two-way ANOVA with Tukey's multiple-comparison test. ****p < 0.0001.

(D–F) BALB/c mice were intranasally challenged with PBS or PBS containing 5×10^5 RB50 or RB50Δ*btrS*. In two individual replicates after RB50Δ*btrS* infection, mice were treated with 15 μL of anti-XCL1 mAb intranasally from day 1–7. Experiments were repeated using the same concentration of anti-XCL1 mAb in a 30-μL volume. On day 7 post infection, lungs were perfused and paraffin embedded. Sections were stained with Hoechst (nucleus, blue), B220 (B cells, red), and CD3 (T cells, green) and imaged using an Olympus CSU W1 spinning disk confocal system. Representative images are shown in (D). To quantify B and T cells, lungs from 6 mice per group were imaged, 3 sections per mouse and 10 ROIs, in the Keyence microscope and quantified with the built-in microscopy software. B cell (E) and T cell (F) counts per ROIs are shown. Each individual point represents the number of positive cells per region of interest in each photo, and the columns represent the mean ± SEM. An outlier test and one-way ANOVA with Dunnett's multiple-comparisons test was performed. *p < 0.01, **p < 0.005, and ****p < 0.0001.

(G) BALB/c mice were intranasally challenged with PBS or PBS containing 5×10^5 RB50 or RB50Δ*btrS*. In two individual replicates after RB50Δ*btrS* infection, mice were treated with 15 μL of anti-XCL1 mAb intranasally from day 1–7. Staining was performed using Hoechst (nucleus, blue), B220 (B cells, red), and PNAd high endothelial venules (green) and imaged using an Olympus CSU W1 spinning disk confocal system to determine the presence of iBALT-specific markers.

Table 1.

Summary of the major findings (RB50/mutant RB50Δ*btrS*)

	Lung clearance (days)	Lung B/T cells (7 dpi)	Mucosal immunity (IgA/Th17)	iBALT (7 dpi)	XCL1 levels
BALB/c	56/14	no/yes	up/high	no/yes	normal/high
C57BL/6J	56/14-21	no/yes	high/very high	no/yes	normal/high
BALB/c ΔdblGATA-1 (no eosinophils)	56/56	no/no	low/low	no/no	low/low
C57BL/6J *EPX/MBP*$^{-/-}$ (no eosinophils)	56/56	no/no	low/low	no/no	low/low

KEY RESOURCES TABLE

REAGENT or RESOURCE	SOURCE	IDENTIFIER
Antibodies		
Zombie Yellow Fixable Viability dye	BioLegend	Cat# 423103
TruStain FcX plus (anti-mouse CD16/32) antibody	BioLegend	Cat# 156604; RRID: AB_2783138
Rat Brilliant Violet 510TM anti-mouse CD45 clone 30-F11	BioLegend	Cat# 103138; RRID: AB_2563061
Rat Brilliant Violet 711TM anti-mouse CD3 clone 17A2	BioLegend	Cat# 100241; RRID: AB_2563945
Rat Alexa Fluor 700 anti-mouse CD19 clone 6D5	BioLegend	Cat# 115528; RRID: AB_493735
Rat Brilliant Violet 785TM anti-mouse CD4 Clone GK1.5	BioLegend	Cat# 100453; RRID: AB_2565843
Rat Alexa Fluor® 488 anti-mouse CD8a Clone 53-6.7	BioLegend	Cat# 100723; RRID: AB_389304
Rat PE/Cyanide 7 anti-mouse INF-y clone XMG1.2	BioLegend	Cat# 505825; RRID: AB_1595591
Rat APC anti-mouse/human IL-5 Clone TRFK5	BioLegend	Cat# 504305; RRID: AB_315329
Rat Brilliant Violet 421TM anti-mouse IL-9 Clone RM9A4	BioLegend	Cat# 514109; RRID: AB_2562728
Rat PE-eFluorTM 610 anti-mouse IL-13 Clone eBio13A	ThermoFisher	Cat# 61-7133-82; RRID: AB_2574654
Rat PerCP/Cyanine5.5 anti-mouse IL-17A Clone TC11-18H10.1	BioLegend	Cat# 506920; RRID: AB_961384
Rat PE anti-mouse IL-33 Clone 396118	ThermoFisher	Cat# MA5-23640; RRID: AB_2606910
Rat Alexa Fluor 488 anti-mouse/human CD11b Clone M1/70	BioLegend	Cat# 101217; RRID: AB_389305
Rat Brilliant Violet 711TM anti-mouse Ly-6G Clone 1A8	BioLegend	Cat# 127643; RRID: AB_2565971
Rat PE anti-mouse SiglecF (CD170) Clone S17007L	BioLegend	Cat# 155506; RRID: AB_2750235
Alexa Fluor 488 anti-mouse CD3 Antibody. Clone 17A2	BioLegend	Cat# 100210; RRID: AB_389301
CD45R (B220) Monoclonal Antibody. Clone RA3-6B2, eBioscience	Invitrogen	Cat# 14-0452-82; RRID: AB_467254
Bone Marrow Proteoglycan (PRG2) Antibody or Major Basic Protein (MBP)	Abbexa	Cat# Abx101775
Purified anti-mouse IgA Antibody, clone RMA	BioLegend	Cat# 407002; RRID: AB_315077
Anti-Mouse XCL1 (Lymphotactin - Biotin)	Leinco Technologies	Cat# L229; RRID: AB_2831159
Rabbit anti-mouse LYVE1 antibody	Abcam	Cat# Ab149117, RRID: AB_301509
Anti-mouse IL17a, clone eBio17B7	ThermoFisher/Invitrogen/ eBioscience	Cat# 13-7177-81; RRID: AB_763570
Anti-mouse PNAd, clone MECA-79	BD Biosciences	Cat# 120802 RRID: AB_395099
Alexa Fluor® 594 donkey anti-rat IgG (H + L)	ThermoFisher Scientific	Cat# A21209: RRID: AB_2535795
Alexa Fluor® 488 goat anti-rabbit IgG (H + L)	ThermoFisher Scientific	Cat# A11008: RRID: AB_143165
Donkey Anti-Rabbit IgG Antibody, HRP conjugate	Millipore-Sigma	Cat# AP182P: RRID: AB_92591
Goat Anti-Rat IgG Antibody, HRP conjugate	Millipore-Sigma	Cat# AP136P; RRID: AB_11214444
Hoechst 33342 Solution	BD Biosciences	Cat# 561908
AF488 Streptavidin conjugate	ThermoFisher/Invitrogen	Cat# S11223
Opal 520 Reagent Pack	Akoya Biosciences	Cat# FP1487001KT: RRID: SKU FP1487001KT
Opal 570 Reagent Pack	Akoya Biosciences	Cat# FP1488001KT
Opal 650 Reagent Pack	Akoya Biosciences	Cat# FP1496001KT
UltraComp eBeads	Invitrogen	Cat# 01-3333-41
Hematoxylin & Eosin stain Kit	Vector Laboratories	Cat# H-3502

REAGENT or RESOURCE	SOURCE	IDENTIFIER
Bacterial and virus strains		
Bordetella bronchiseptica RB50 strain	Cotter et al., 1994[36]	PMID: 8039908
Bordetella bronchiseptica RB50Δ*btrS* strain	Mattoo et al., 2004[37]	PMID: 15130135
Bordetella bronchiseptica RB50Δ*bscN* strain	M. H. Yuk et al., 2000[114]	PMID: 9663681
Biological samples		
Bone marrow derived eosinophils	E. Mai et al., 2021[74]	PMID: 33486726
Chemicals, peptides, and recombinant proteins		
rmFLT3L	PrepoTech	Cat# 250-31L
rmSCF	PrepoTech	Cat# 250-03
IL-5	PrepoTech	Cat # 215-15
ProLong Glass Antifade Mountant	ThermoFisher/Invitrogen	Cat# 36984
Isoflurane	Attane	Cat# RXISO-250
Paraformaldehyde, EM Grade, Purified Granular	Electron microscopy sciences	Cat# 19210; CAS #30525-89-4
PBS, pH 7.4	ThermoFisher/Gibco	Cat# 10010031; Identifier: 10010-049
Trizol Reagent	ThermoFisher/Ambion Life Technologies	Cat# 15596018
RNAse Zap RNAse decontamination solution	ThermoFisher/Invitrogen	Cat# AM9782
Bordet-Gengou Agar	VWR/BD Life Sciences	Cat# 90003-414
Streptomycin sulfate	ThermoFisher/Gibco	Cat# 11860038; Identifier: 11860-038
LB Broth	Fisher Scientific	Cat# BP1426-500
Xylene	Azer Scientific	Cat# E5609
Triton X-100	VWR/BD Life Sciences	Cat# 9002-93-1
Normal Goat Serum	Vector Technologies	S-1000
Bovine Serum Albumin	Fisher Scientific	Cat# BP9703-100
ACK Lysis buffer	ThermoFisher/Gibco	Cat# A1049201
Lung dissociation kit	Miltenyi Biotech	Cat# 130-095-927
RPMI	ThermoFisher/Gibco	Cat# 11875119
Fetal Bovine Serum	ThermoFisher/Gibco	Cat# 10437028
beta-mercaptoethanol	Sigma	Cat# 60-24-2
Cell activation cocktail containing brefeldin A	BioLegend	Cat# 423304
Dynabeads CD3/CD28	ThermoFisher/Invitrogen	Cat# 11452D
Critical commercial assays		
PureLink RNA Extraction kit	Invitrogen	Cat# 2365053
Qubit RNA assay	Denovix	Cat# DS-11 FX
TapeStation D1000 assay	Agilent Technologies	Cat #50675582
LUNA One-Step qRT-PCR Kit	New England Biolabs	Cat #E3005L
Thelper v13 LegendPlex Chemokine ELISA	BioLegend	Cat#740451
Thelper v13 LegendPlex Cytokine ELISA	BioLegend	Cat#741044
GentleMacs Dissociator Mouse Lung Dissociation Kit	Miltenyi Biotech.	Cat#130-095-927
MojoSort™ Mouse CD3$^+$ T cell Isolation Kit	BioLegend	Cat#480024
Dynabeads™ Mouse T-Activator CD3/CD28 T cell Expansion and Activation Beads	Gibco	Cat #11456D

REAGENT or RESOURCE	SOURCE	IDENTIFIER
NEBNext® Library Quant Kit for Illumina®	New England Biolabs	Cat# E7630L
Stranded mRNA Prep Ligation kit	Illumina	Cat# 20040532
PureLink DNase Set	Invitrogen	Cat #12185010
Deposited data		
FASTQ files	EMBL-EBI (https://www.ebi.ac.uk/biostudies/arrayexpress/studies/E-MTAB-13332); LSU Health Sciences Center at Shreveport	BioStudies: E-MTAB-13332
Mus musculus reference genome version GRCm39	Genome Reference Consortium (GRC)	GenBank: GCA_000001635.9
Mus musculus gene transfer format (.gtf) annotated version GRCm39.105: GCA_000001635.9	NCBI RefSeq	RefSeq: GCF_000001635.27-RS_2023_04
Experimental models: Cell lines		
Murine bone marrow-derived eosinophils	Mai et al., 2021[74]	PMID: 33486726
Experimental models: Organisms/strains		
Mouse: BALB/cJ	Jackson Laboratories	Cat# 000651; RRID: IMSR_JAX:000651
Mouse: ΔdblGATA: B6.129S1(C)-Gata1tm6Sho/LvtzJ	Jackson Laboratories	Cat# 033551; RRID: IMSR_JAX:033551
Mouse: C57BL/6J	Jackson Laboratories	Cat# 000664; RRID: IMSR_JAX:000664
Mouse: EPX/MBP$^{-/-}$: MBP-1−/−/EPX$^{-/-}$	Donation from Dr Jacobsen La Joya	PMID: 28515227
Oligonucleotides		
b-Actin Fw	IDT (Integrated DNA Technologies)	PMID: 31889098
b-Actin Rv	IDT (Integrated DNA Technologies)	PMID: 31889098
Il-17 Fw	IDT (Integrated DNA Technologies)	PMID: 17918201
IL-17 Rv	IDT (Integrated DNA Technologies)	PMID: 17918201
IFNγ Fw	IDT (Integrated DNA Technologies)	PMID: 23133493
IFNγ Rv	IDT (Integrated DNA Technologies)	PMID: 23133493
CCL-19 F	IDT (Integrated DNA Technologies)	PMID: 19651862
CCL-19 Rv	IDT (Integrated DNA Technologies)	PMID: 19651862
MadCam-1-Fw	IDT (Integrated DNA Technologies)	PMID: 31526758
MadCam-1-Rv	IDT (Integrated DNA Technologies)	PMID: 31526758
Software and algorithms		
LegendPlex™ Data Analysis Software Suite	Qognit	legendplex.qognit.com
Keyence Image Analysis Software (version 1.1.2)	Keyence Corporation America	Cat# BZ-H4A, BZ-H4M, BZ-H4CM, BZ-H4R
qRT-PCR fold-change mRNA expression	The Ultimate qPCR Experiment: Producing Publication Quality, Reproducible Data the First Time: Trends in Biotechnology (cell.com)	PMID: 30654913

REAGENT or RESOURCE	SOURCE	IDENTIFIER
Illumina NovaSeq Control Software v1.7.5; RTA v3	https://support.illumina.com/downloads/novaseq-control-software-v1-7-5.html	V 1.7.5; RTA v3
Trimmomatic adaptor (version 0.38)	https://github.com/usadellab/Trimmomatic/tree/main	V 0.38
DESeq2 R package (version 1.34.0)	https://doi.org/10.18129/B9.bioc.DESeq2	V 1.34.0
Cluster profiler package (version 4.2.2)	https://doi.org/10.18129/B9.bioc.clusterProfiler	V 4.2.2
ashr' shrunkage package	https://github.com/stephens999/ashr	N/A
RSEM software (version 1.3.1)	https://deweylab.github.io/RSEM/	V 1.3.1
STAR RNA-Seq Read Mapper (version 2.7)	https://github.com/alexdobin/STAR; https://doi.org/10.1093/bioinformatics/bts635	V 2.7
FlowJo (version 10.9)	TreeStar, Ashland, OR	V 10.9
GraphPad (version 10.0.2)	https://www.graphpad.com	V 10.0.2
Other		
Bulk cartridge CodePlex Secretome	IsoPlexis	Cat# CodePlex Inflammation-L Chip 2, CODEPLEX-@L-10-2
All-in-One Fluorescence Microscope	Keyence	Cat# BZ-X810
CFX96 Touch Real-Time PCR	Bio-Rad	Cat# CFX96 Touch Real-Time PCR Detection System
NovaSeq 6000	Illumina	Model: Illumina NovaSeq 6000
BaseSpace Sequence Hub	Illumina	https://www.illumina.com/products/by-type/informatics-products/basespace-sequence-hub.html
NovoCyte Quanteon Flow Cytometer	Agilent	Cat#64-1-1812-1046-4
GentleMACS Octo Dissociator with Heaters	Miltenyi Biotech	Cat# 130-096-427
NanoDrop One-C	NanoDrop	Serial #A241601534
Countess 3 Automated Cell Counter	Invitrogen	Cat #AMQAX2000
Bead Mill Homogenizer 120V (25 mL-5mL)	VWR-Avantor	Cat#75840-022
DeNovix DS-11 FX Spectrophotometer	Qubit	https://www.denovix.com/products/ds-11-fx-spectrophotometer-fluorometer/
2 mL reinforced Bead Mill tubes	VWR-Avantor	Cat# 10158-556
0.4 mm glass beads	VWR-Avantor	Cat# 12621-154
1.4 mm ceramic beads	VWR-Avantor	Cat# 10158-552
Hard-Shell PCR Plates 96-well, thin wall	Bio-Rad	Cat# HSP9601
Microseal B seals	Bio-Rad	Cat# MSB1001
Miltenyi dissociation tubes	Miltenyi Biotech	Cat# 130-095-927
40μm filters	Falcon	Cat# 352340
Keyence BZ-X800E	Keyence Corporation	Cat# BZ-X800E